Backbone analysis for nonlinear vibrations in rotor dynamics

Alexander D. Shaw*, Mehmet S. Akay, Michael I. Friswell
Department of Aerospace Engineering, Swansea University, UK
*Corresponding author: a.d.shaw@swansea.ac.uk

March 6, 2026

Abstract

Backbone curves are a well established practice for understanding the vibrations of nonlinear structures, by charting the frequency-amplitude relations for the underlying conservative system. However, in their typical form they are ineffective in tracing many of the phenomena seen in the lateral vibrations of an isotropically supported rotating disk, which include both periodic, quasiperiodic and isolated responses. This is because the underlying conservative system lacks mechanisms to drive the mode locking that is an essential part of these responses. However, to include effects such as unbalance forcing that can induce these behaviours would reduce the generality of the analysis, and may also require knowledge of parameters that can be difficult to control or measure. This work produces backbone curves with additional constraints to ensure that the response remains in phase with the unbalance forcing, acting in the place of the physical causes of mode locking. These curves provide a skeleton that sits underneath the bifurcation diagrams of a wide range of nonconservative and also weakly anisotropic rotating disc systems, despite being calculated with just the underlying conservative and isotropic parts of the system. This allows a systematic means of exploring the complex response space of rotating systems, enabling continuation approaches to efficiently find isolated response regions that previously required a sweep of many time simulations to discover. The approach provides some commonality to the analysis of a diverse range of responses. The method is demonstrated on an isotropic 2 degree of freedom overhung rotor with a smooth radial stiffness nonlinearity, but is shown to have relevance to nonsmooth systems and weakly anisotropic systems. An experimental comparison is also given.

1 Introduction

1.1 Rotating machines

Machines with rotating elements play a ubiquitous role in engineering, from turbomachinery for aircraft engines and power generation, through to electrical devices including motors and generators. Understanding their vibrations is crucial to maintaining a long service life, efficient performance, avoiding harmful resonant behaviour and being able to detect faults which may arise [1].

Understanding the role that nonlinearities play in the lateral vibrations of such system is a vital yet challenging area, with much research still ongoing, for example [2, 3, 4, 5, 6, 7]. Nonlinearities occur due to effects such as contact between rotating parts and a surrounding stator [8, 9], fluid interactions [10, 11], bearing dynamics [12, 13] and geometric stiffness nonlinearity [14, 15]. These physical effects lead to complex vibration responses that cannot be modelled through simple linear responses, including amplitude dependent natural frequencies, jump phenomena, harmonic and subharmonic frequency content (relative to the drive speed), chaotic and quasiperiodic behaviour [16]. A particular problem is the possibility of isolated regions of quasiperiodic responses, which can lead to large amplitude limit cycles,

and occur at drivespeeds substantially removed from where direct resonances would be expected [8, 17]. These responses are experimentally challenging, because they require particular initial conditions to be active, and therefore their existence can easily be missed by conventional run up or run down tests.

The problem of finding appropriate initial conditions also makes these responses awkward to handle numerically,with a common approach being to perform a large number of time simulations with various initial conditions, and this process must typically be repeated over a range of different drive speeds [17, 18]. These time simulations sometimes need to integrate stiff equations of motion, and the result is that even quite small systems can be expensive and time consuming to characterise numerically. Sample and basin stability methods offer a more sophisticated approach, but still have the requirement for many potentially slow time simulations [19, 20].

It follows that a means of path following, from low amplitude solutions that are easily modelled up to these isolated solutions, would be invaluable, but to the author's knowledge this does not presently exist. In works by Akay *et al.* [21, 22] numerical continuation was used but it was found that the connection between limit cycles and lower amplitude responses only existed in the limit of zero excitation and damping, at which point the required modal interactions and nonlinear forces become negligible as well. This creates a numerical barrier to progressing a solution from low amplitude to a high amplitude limit cycle. Therefore, while continuation works well to trace a family of responses once an initial solution had been found, a systematic and reliable means of locating this initial solution is required.

Many authors have made substantial progress on this specialised form of vibration analysis. Ehrich compiled many works on vibration phenomena seen in turbomachinery both experimentally and numerically, for example [23, 24, 25] with a good summary in [26]. As early as 1955, there are papers by Yamamoto discussing issues such as subharmonics and clearance nonlinearity, although the present authors have not been able to access these papers as they are in Japanese. However, this work continued with many works by Ishida and Inoue *et al.* , highlighting both experimentally and analytically the role of internal resonance, in particular the $-1:1$ resonance near the critical speed [15, 27, 28, 29], and the potential for chaotic oscillations [30]. Muszyńska described many experimental observations of both real machines and experimental test rigs including all manner of bearing, contact and fluid phenomena, with associated analysis in both frequency and time domains with insights for fault diagnosis; these works could justify a substantial review paper on their own, but fortunately they are summarised in [31]. An interesting paper by Neilson and Barr [32] concerning a rotor with a piecewise nonlinearity in the support stiffness highlighted the presence of frequency content unrelated to the drive speed and aperiodic responses, although it also highlighted that these appeared to be perfectly periodic in polar coordinates (a theme resumed herein). Many authors began to relate these phenomena from nonlinear dynamical theory, for example [33, 25, 34, 35] describing various phenomena in terms of bifurcations, chaos and subharmonic resonance. There have also been numerous modified harmonic balance approaches applied to various responses by Kim and Noah [36, 37], von Groll and Ewins [38], Salles *et al.* [39] and Shaw *et al.* [40]. Peletan *et al.* applied harmonic balance with two base frequencies in order to capture quasiperiodic behaviour [41]. A key aspect to the complexity of responses is that they are typically multi-modal, and furthermore mode locking is a fundamental feature of many responses. This aspect was explored in detail by van der Heijden [42] with an analysis of a system representing a loose bearing, highlighting how the mode locking typically occurs in a system corotating with the shaft, and also showing how perturbing the full rotational symmetry[1] substantially changes the nature of responses.

Due to the typically harsh nature of rotor-stator contacts, Cole, Keogh, Mora and others have used an impact mapping approach, where velocity instantly changes at the occurunce of contact, rather than creating a nonlinear forcing function [43, 44, 45], and despite the substantially different modelling ap-

[1] In more common rotordynamics terms, this would be described as changing from an isotropic system to an anisotropic one.

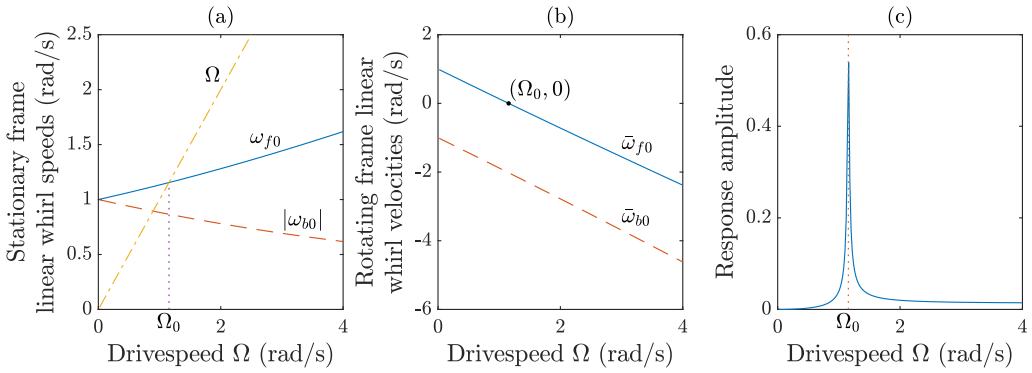

Figure 1: (a) Campbell diagram showing stationary frame natural frequencies of the linear part of system (1) against drivespeed Ω. (b) Rotating frame whirl velocities against Ω. (c) Response amplitude of system $\mathbf{M}\ddot{\mathbf{x}} + (\Omega\mathbf{G} + \mathbf{C})\,\dot{\mathbf{x}} + \mathbf{K}\mathbf{x} = \varepsilon\Omega^2 \begin{bmatrix} \cos\Omega t \\ \sin\Omega t \end{bmatrix}$. All plots use parameters from Table 1 except for $k_3 = 0$; for plot (c) $\mathbf{C} = \begin{bmatrix} 0.02 & 0 \\ 0 & 0.02 \end{bmatrix}$ and $\varepsilon = 0.01$.

proach similar rotating frame mode locking was demonstrated. These papers highlight an important distinction in rotating machinery dynamics, that of synchronous as opposed to asynchronous oscillations. Synchronous oscillations demonstrate stationary frame periodicity and frequency content commensurate with the drivespeed. Asynchronous oscillations appear quasiperiodic in the stationary frame, with frequency content that is not commensurate with the drivespeed, but are periodic in the corotating coordinate system. Zilli *et al.* [8] explained the onset of quasiperiodic responses somewhat differently, in terms of angular synchronisation between the unbalance forcing and the underlying frequencies. In this way, a minimum drivespeed for certain forms of quasiperiodic responses to occur was defined in terms of the underlying linear frequencies of the system. This condition was developed by Shaw *et al.* for higher dimensional systems, and shown to be equivalent to an internal resonance condition in the rotating frame.

There has been some application of nonlinear normal mode (NNM) and manifold methods to rotating systems [46, 47, 48]. Legrand *et al.* created a nonlinear normal mode (in the form of an invariant manifold) of a rotating shaft with oil film nonlinearity to describe its decaying free oscillations [49]. This used an intriguing method to deal with complex mode shapes, although could not model multimode behaviour that arose at certain drive speeds. Wang and Ding [50] described an NNM approach to balancing a nonlinear rotor that was also subject to gravity sag. This demonstrated the benefits of a nonlinear approach to balancing, although gyroscopics were not considered. Wang *et al.* calculated a low order approximation of a spectral submanifold for a rotor-stator rub system [51], including cross-stiffness effects due to fluid bearing effects and friction, finding that the model worked well for relatively light forcing. Rotating beams have been considered with these methods using both classical PDE formulations [52] and finite element techniques [53]. Martin *et al.* used direct parametrisation to derive invariant manifolds for both rotating beams and plates [54]. Mereles *et al.* created a reduced order model of a high dimensional rotor system with quite realistic foundation modelling using the approximate invariant manifold method [55]. The same authors used a centre manifold approach to model the fluid film nonlinearity [56]. However to the author's knowledge, NMM methods have not yet captured the full complexity of response seen in works such as [8, 17] and other works cited above, and it is hoped that the present work can facilitate future work in this area by better understanding of the paths to isolated resonances.

1.2 Aspects of vibration particular to rotordynamics

In the present work the vibrations of an isotropically supported rotating disc are considered, and these have some important differences to those of static structures. In the linear case, the dynamics are characterised by eigenvalues that are repeated at zero drivespeed, that then diverge from each other as drivespeed increases, due to gyroscopic effects. This effect is illustrated in Figure 1 (a), which shows an example of the Campbell diagram that is traditionally used to illustrate how natural frequencies vary with drive speed. The modal responses of this system consist of circular orbits, where the mode labelled ω_{f0} in Figure 1 is known as a forward whirl because it orbits in the same direction as the shaft rotation. The other mode denoted ω_{b0} is known as a backward whirl because it orbits in the opposite direction to the shaft rotation [1]. This directional property of the modes means that the frequencies of the system can be properly thought of as angular velocities, and given negative signs if backward whirling. It is often useful to perform analysis in a coordinate frame that is rotating with the shaft, and the use of signed angular velocities means that whirling velocities are easily found in this frame simply by subtracting the shaft speed, giving $\bar{\omega}_{f0}$ as $\bar{\omega}_{b0}$ shown in Figure 1 (b)[2]. The rotating frame whirl speeds vary strongly with drivespeed, even if the gyroscopic effects are weak, and this allows many different integer ratios between angular velocities to be achieved by varying drive speed.

A practical consideration in analysis of rotating systems is that the primary form of excitation is unbalanced mass on the shaft exerting a force vector that rotates at the drivespeed, which leads to important differences in behaviour compared to the harmonic excitation typically considered for static structures, and this again can be seen in a linear system. Figure 1 (c) shows a typical response of a damped rotordynamic system to unbalance forcing. The figure shows a single peak, as the drive speed passes the condition value $\Omega = \omega_{f0} = \Omega_0$, where Ω_0 is the linear critical speed [1]. There is no peak due to the backward whirling mode, and it can be shown that the backward whirl motion cannot be forced by the forward rotating unbalance force vector for a system with isotropic supports [1] .

In the nonlinear case, the use of signed rotational velocities as opposed to unsigned frequencies can mean that complex Fourier analysis is needed to capture harmonics in analysis [40]. It also allows modal interactions with negative frequency ratios such as -1:1, where a backward whirl is being excited by a forward whirl [30]. The variation in underlying linear frequencies with drivespeed means that many different forms of mode locked response can occur, and hence drivespeed not only determines the excitation but also the forms of modal interaction that can occur. The mode locking is in many cases seen in a coordinate system that rotates with the shaft, leading to responses that are periodic within this rotating frame, whilst being generally aperiodic in the stationary frame. Some multimode responses are seen where neither of the active modes are at the frequency of the unbalance forcing, occuring at drivespeeds well above the linear critical speed, and making no connection with directly excited resonances [17].

Thus far, there have been calculations of these responses in the forced and damped case, and the consideration of underlying linear modes has been used to derive a lower bound for drivespeed where such responses are possible [40, 8, 17]. However, a more complete explanation of why and where these resonant responses appear seems to be lacking from the literature.

Another awkward problem is that these resonant responses only seem to connect to the low level (ie. linear) behaviour of the system in the limit of zero forcing and damping. However, the physical causes of mode locking seem to occur within the nonconservative parts of the system, and if the system is reduced to only its conservative parts many of the above behaviours cease to occur. This is in contrast to many vibrating systems where the conservative analysis provides invaluable insight into the broader behaviours of the system.

The above characteristics mean that rotating systems under unbalance forcing provide some important

[2]If unsigned frequencies are used, more complex sum and difference frequency relations are seen.

differences in approach to existing nonlinear vibration methodologies. To summarise, these are:

1. The possibility of mode locking in either or both of stationary and rotating coordinate systems.
2. The existence of response branches that appear wholly disconnected from direct resonances. (Section 5.5.3 will show that the responses grow from a combination of linear modes that only exists at a particular drive speed.)
3. The typically considered unbalance forcing means that drivespeed is a crucial parameter affecting excitation and the underlying linear frequencies, and hence that modal excitation is less straightforward.
4. Some computational challenges from requirements for signed frequencies and complex Fourier analysis if working in the frequency domain.
5. In many practical cases, such as rotor-stator contact, the nonlinearities are nonsmooth.

1.3 The present work: Backbone curves for rotating systems

A widely used concept in the nonlinear structural dynamics of nonrotating systems is the backbone curve, generally defined as the relationship between amplitude and frequency. More specifically, this work considers backbone curves defined for free vibrations of the underlying conservative systems[57], as opposed to those found from the instantaneous frequency content of decaying vibrations[58]. Such curves sit beneath the forced responses of the full nonconservative system, giving great insight over a range of excitation and damping conditions in an efficient way. They can deal with complex multi-modal structures featuring internal resonances; in some cases these internal resonances reveal characteristic 'loops' in the backbone curve which strongly indicate the regions where there is potential for effects such as jump phenomena, torus bifurcations, and saturation in the forced response [59, 60, 61].

The conservative approach to backbone curves serves rotating systems poorly in its present form. As will be shown in Sections 3 and 4, in the conservative isotropic system mode locking does not occur, and therefore many of the more complex mode locked responses seen in nonconservative systems are not predicted. This leads to the problem discussed in Section 1.2 where some responses are isolated in the nonconservative system, but degenerate in the conservative system.

This paper shows a variation on the conservative backbone approach allowing it to reveal a broad range of nonlinear responses of rotating systems. A simple rotor system with a smooth nonlinearity is used as a case study, the equations of motion for the underlying istropic conservative system are derived, and responses found. The physical effects that lead to mode locking are shown to be absent in this system, but they are replaced with mathematical constraints that reduce the solution space to only those responses that may be excited by unbalance forcing, which is the principle concern in rotating systems. It is shown that this relatively simple approach reveals so called 'constrained backbones' that underpin the nonlinear responses of various nonconservative system. Furthermore, the responses are connected to much simpler, constant amplitude responses so that they may be found with a systematic continuation procedure, without the need to guess suitable initial conditions for simulation or a start value for a numerical solver. The backbones are derived firstly at constant drivespeeds, revealing bounded solution branches of bouncing solutions, which can then be used to place an approximate envelope on the amplitudes of a bifurcation diagram plotted against drive speed for a fully forced and damped system.

Section 2 introduces the conservative system to be analysed, then Section 3 gives the general responses of this system, showing them to be essentially simple, but in most cases this analysis is of little practical value on its own. Section 4 derives the backbone curves of the constant amplitude whirling solutions using a fixed point analysis, as these are essential to be able to continue from a low amplitude to the

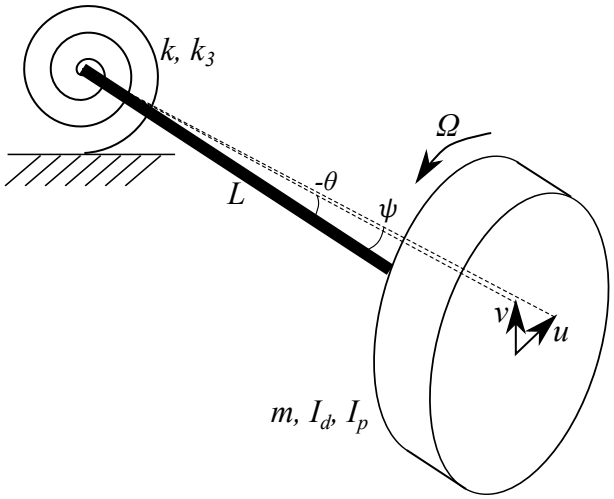

Figure 2: An isotropic conservative rotor system with nonlinear radial stiffness.

onset conditions of more complex orbits. Section 5 then shows how to trace backbones for different types of variable amplitude bouncing orbits. The resulting constrained backbones for the conservative isotropic system are then compared to simulations of systems additionally including forcing, damping and perhaps anisotropy in Section 6. Section 7 demonstrates the method against an experiment, and conclusions are drawn in Section 8.

2 System definition

The system is shown in Figure 2. A disc is mounted at one end of a rigid shaft of length L, that is rotating at constant speed Ω rad/s. The shaft is mounted at its other end to a nonlinear rotational spring, and therefore the motion of the disc centre can be described either by angles ψ and θ about the support or by centre translations u and v, where $u = L\psi$ and $v = -L\theta$ for $u, v \ll L$. The spring generates a restoring moment, that may be equivalently represented by a restoring force applied at the disc centre given by $\left[ku + k_3 r^2 u, v + k_3 r^2 v\right]^T$, where $r^2 = u^2 + v^2$.

Following [1] the disc has mass m, diametral moment of inertia I_d and polar moment of inertia I_p. Rotations of the disc will induce inertial moments $-I_d[\ddot{\theta}, \ddot{\psi}]^T$ and gyroscopic moments $\Omega I_p[\dot{\psi}, -\dot{\theta}]^T$, which again may be represented by equivalent forces acting at the disc centre by dividing through by L.

Representing the motion of the disc in terms of translations u and v, including the above equivalent forces and the kinematic relations between translations and rotations, we obtain the equation of motion

$$\mathbf{M}\ddot{\mathbf{x}} + \Omega\mathbf{G}\dot{\mathbf{x}} + \mathbf{K}\mathbf{x} + k_3 r^2 \mathbf{x} = \begin{bmatrix} 0 \\ 0 \end{bmatrix} , \tag{1}$$

where

$$\mathbf{x} = \begin{bmatrix} u \\ v \end{bmatrix}, \mathbf{M} = \begin{bmatrix} M & 0 \\ 0 & M \end{bmatrix}, \mathbf{G} = \mu \begin{bmatrix} 0 & 1 \\ -1 & 0 \end{bmatrix}, \mathbf{K} = \begin{bmatrix} k & 0 \\ 0 & k \end{bmatrix}$$

and $r^2 = \mathbf{x}^T\mathbf{x}$, $M = m + \frac{I_d}{L^2}$ is the effective mass, and $\mu = \frac{I_p}{L^2}$. As such the system is the simplest case of a conservative system with the essential features of nonlinearity, gyroscopics and isotropy. The nonlinearity could approximate any smooth nonlinearity in a rotating system, for example bend stretch coupling of a flexible shaft. Gravity is neglected.

It is also useful to consider the system in a coordinate system that rotates at speed Ω around the

Table 1: Nondimensional system parameters used throughout Sections 3, 4 and 5.

M	k	k_3	μ
1	1	1	0.25

origin, giving the relation $\bar{\mathbf{x}} = [\bar{u}, \bar{v}]^T = \mathbf{T}(\Omega, t)\mathbf{x}$ where

$$\mathbf{T}(\Omega, t) = \begin{bmatrix} \cos\Omega t & \sin\Omega t \\ -\sin\Omega t & \cos\Omega t \end{bmatrix} . \tag{2}$$

Noting that $(\mathbf{T}(\Omega, t))^{-1} = (\mathbf{T}(\Omega, t))^T$, and applying chain and product rules results in the transformed equation of motion

$$\mathbf{M}\ddot{\bar{\mathbf{x}}} + \Omega\bar{\mathbf{G}}\dot{\bar{\mathbf{x}}} + \bar{\mathbf{K}}\bar{\mathbf{x}} + k_3 r^2 \bar{\mathbf{x}} = \begin{bmatrix} 0 \\ 0 \end{bmatrix} , \tag{3}$$

where

$$\bar{\mathbf{G}} = \mathbf{G} - 2\mathbf{M}\mathbf{J}, \quad \bar{\mathbf{K}} = \mathbf{K} - \Omega^2\mathbf{M} - \Omega^2\mathbf{G}\mathbf{J} \quad \text{and} \quad \mathbf{J} = \begin{bmatrix} 0 & 1 \\ -1 & 0 \end{bmatrix} .$$

A further view of the system is the first order polar representation $\mathbf{y} = [r, \alpha, \dot{r}, \dot{\alpha}]^T$ where

$$r = \sqrt{u^2 + v^2} \ , \ \dot{r} = \frac{u\dot{u} + v\dot{v}}{r} \ , \ \dot{\alpha} = \frac{-\dot{u}v + \dot{v}u}{r^2} \ , \tag{4}$$

and α is found by integration of $\dot{\alpha}$ with respect to time. In order to maintain smoothness, α is not restricted to any range such as $0 \leq \alpha < 2\pi$. The reverse transforms are

$$u = r\cos\alpha \ , \ v = r\sin\alpha \ , \ \dot{u} = \dot{r}\cos\alpha - r\dot{\alpha}\sin\alpha \ , \ \dot{v} = \dot{r}\sin\alpha + r\dot{\alpha}\cos\alpha \ .$$

The state space equation of motion in polar form is

$$\dot{\mathbf{y}} = \begin{bmatrix} 0 & 0 & 1 & 0 \\ 0 & 0 & 0 & 1 \\ \frac{-k}{M} & 0 & 0 & 0 \\ 0 & 0 & 0 & 0 \end{bmatrix} \mathbf{y} + \begin{bmatrix} 0 \\ 0 \\ \frac{-k_3 r^3}{M} - \frac{\mu\Omega}{M} r\dot{\alpha} + r\dot{\alpha}^2 \\ \frac{-2\dot{r}\dot{\alpha}}{r} + \frac{\mu\Omega\dot{r}}{Mr} \end{bmatrix} = \mathbf{f}_\mathbf{p}(\mathbf{y}) . \tag{5}$$

Finally, since the system is isotropic, true understanding of its fundamental behaviour comes in a coordinate frame that is truly agnostic of the angular position of the disk (α). Noting that in Eq. (5) no other states are driven by α, we can reduce $\mathbf{y}$ to $\hat{\mathbf{y}} = [r, \dot{r}, \dot{\alpha}]^T$ with equation of motion

$$\dot{\hat{\mathbf{y}}} = \begin{bmatrix} 0 & 1 & 0 \\ \frac{-k}{M} & 0 & 0 \\ 0 & 0 & 0 \end{bmatrix} \hat{\mathbf{y}} + \begin{bmatrix} 0 \\ \frac{-k_3 r^3}{M} - \frac{\mu\Omega}{M} r\dot{\alpha} + r\dot{\alpha}^2 \\ \frac{-2\dot{r}\dot{\alpha}}{r} + \frac{\mu\Omega\dot{r}}{Mr} \end{bmatrix} = \mathbf{f}_\mathbf{a}(\hat{\mathbf{y}}) . \tag{6}$$

Equations (1), (3), (5) and (6) are herein referred to respectively as the stationary, rotating, polar and agnostic equations of motion.

3 General responses of the isotropic system

In this section and in Sections 4 and 5, it is assumed without loss of generality that the system has been defined in a set of units that allows the parameters to become the convenient nondimensional values found in Table 1.

3.1 Response in polar or agnostic coordinates

Figure 3 shows the flow of the system for arbitrary initial values of r and $\dot{\alpha}$. It may be seen that the agnostic system shows a simple oscillating behaviour with period T, and it is shown that this is the only possible behaviour (besides a fixed point) in Appendix A. The polar system has no form of periodicity, due to α, but does reveal a useful property of a period in the agnostic system, namely the precession angle $\Psi = \alpha(t+T) - \alpha(t)$, which is the total change in α during T.

3.2 Response in stationary or rotating coordinates

When projected into other coordinate systems, the response looks far more complicated as seen in Figure 3(b), where the trajectory will only repeat if Ψ is a rational fraction of 2π. The behaviour is generally quasiperiodic, where T can be thought of as the 'quasiperiod'. The position vector performs a pure rotation about the origin every quasiperiod; in the stationary frame this can be written as

$$\mathbf{x}(t+T) = \begin{bmatrix} \cos\Psi & -\sin\Psi \\ \sin\Psi & \cos\Psi \end{bmatrix} \mathbf{x}(t) \; .$$

Similarly, the rotating frame trajectory in Figure 3(c) is in general quasiperiodic and nonrepeating.

The flow can become periodic in either the stationary or rotating frames, if Ψ satisfies certain criteria. For stationary frame periodicity, this implies that

$$p\Psi = q2\pi \; , \tag{7}$$

and for rotating frame periodicity

$$p(\Psi - \Omega T) = q2\pi \; , \tag{8}$$

where p and q are integers. Equation (8) can be thought of as a generalisation of the angular synchronisation condition proposed in [8], allowing the whirling velocities to vary in a nonlinear manner instead of using the linear predictions, and using signs to indicate whether whirling is backward or forward.

Note that there is nothing in the dynamics of the conservative system to enforce conditions (7) or (8). Given that the agnostic response does not bifurcate from simple oscillatory behaviour, it may be concluded that Ψ and T will vary smoothly with changes to initial conditions, giving periodicity in stationary or rotating coordinate frames only for particular initial conditions. If the general response in stationary or rotating coordinate systems is considered to be composed from the two underlying modes, this shows that there is no meaningful locking between the modes to enforce periodicity in these coordinate systems.

4 Constant amplitude backbone curves

4.1 Forward and backward whirling

When the initial conditions are at a fixed point of system (6), the stationary frame orbit will be circular, and the rotating frame will show a circular orbit or a fixed point. The fixed points of system (6) have the form

$$\hat{\mathbf{y}}^* \;=\; \begin{bmatrix} r \\ 0 \\ \omega_f(r,\Omega) \text{ or } \omega_b(r,\Omega) \end{bmatrix} \quad \text{where} \quad \omega_f(r,\Omega), \omega_b(r,\Omega) \;=\; \frac{\Omega\mu}{2M} \pm \sqrt{\left(\frac{\Omega\mu}{2M}\right)^2 + \frac{k + k_3 r^2}{M}} \quad . \tag{9}$$

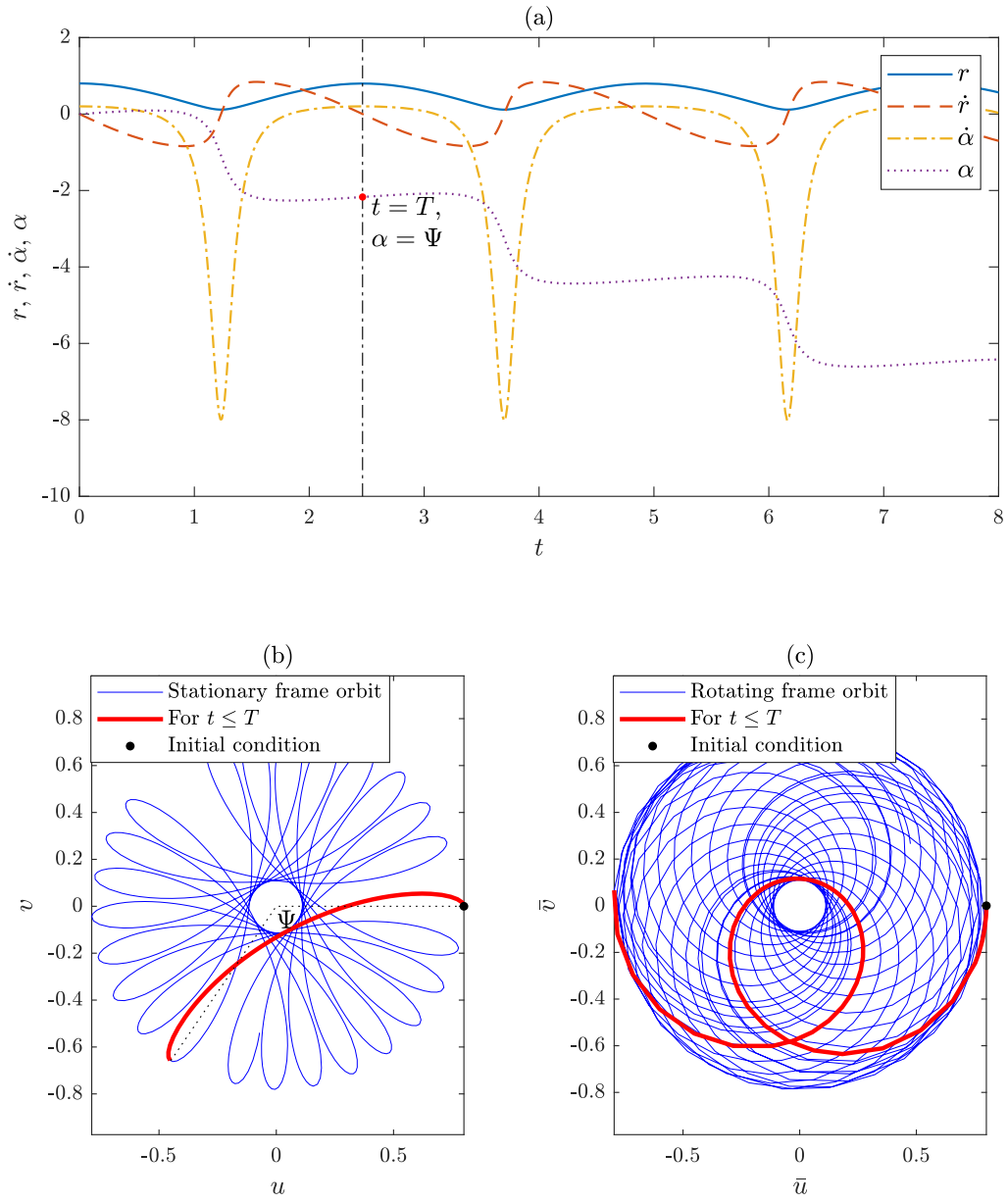

Figure 3: Three different views of a typical response of the isotropic conservative rotor. $\Omega = 3$. At $t = 0$, $r = 0.8$, $\dot{r} = \alpha = 0$, and $\dot{\alpha} = 0.2$, with other parameters given in Table 1.

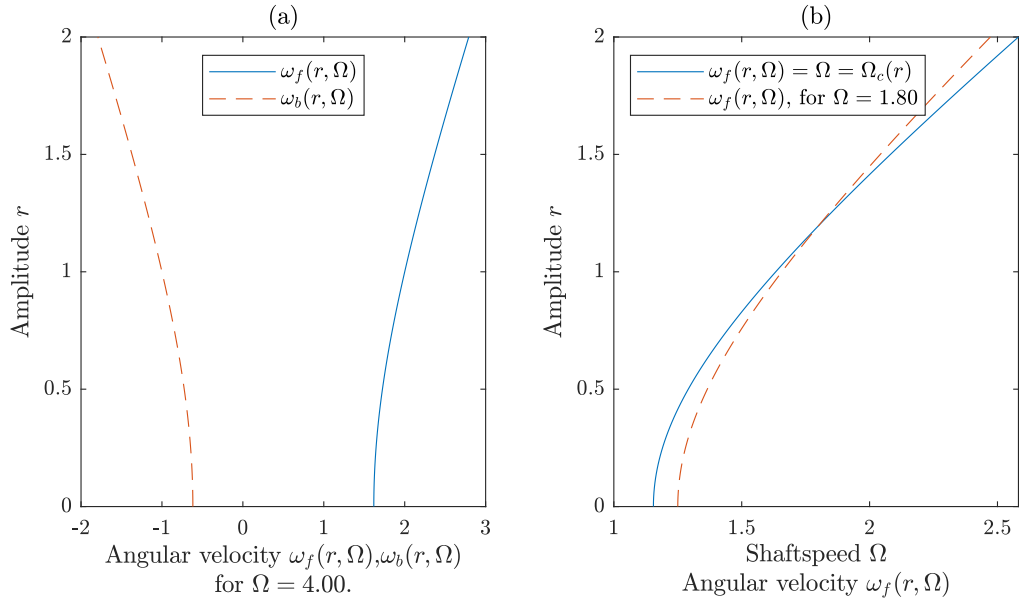

Figure 4: (a) Amplitude dependent whirl angular velocities for $\Omega = 4$, calculated with Eq. (9). (b) Critical speed backbone curve (solid) as given by equation (11), with the constant amplitude backbone for forward whirl $\omega_f(r, 1.8)$ added for comparison (dashed).

Equation (9) gives the amplitude dependent angular frequencies $\omega_f(r,\Omega)$ and $\omega_b(r,\Omega)$ of the forward and backward whirling solutions, which are circular orbits with radius r and the given angular velocities in the stationary frame. Figure 4 (a) plots the relationship between these angular frequencies and amplitude for a typical system; note that $\omega_b(r,\Omega)$ is negative as it represents a clockwise motion in the stationary frame, whereas $\omega_f(r,\Omega)$ is positive and represents an anticlockwise motion[3].

The equivalent angular velocities viewed in the rotating frame are obtained by subtracting the drivespeed to give

$$\bar{\omega}_f(r,\Omega) = \omega_f(r,\Omega) - \Omega \quad , \quad \bar{\omega}_b(r,\Omega) = \omega_b(r,\Omega) - \Omega \; . \tag{10}$$

As amplitude tends to zero, it can be be seen that $\omega_f(r,\Omega)$ and $\omega_b(r,\Omega)$ tend to the well known forward and backward whirl solutions of the linear part of Eq. (1), and therefore these solutions can be considered to be nonlinear extensions of the linear modes. The curves in Figure 4 (a) can also be considered to be backbone curves, and we term them here the *forward whirl backbone* and *backward whirl backbone* curves respectively. However, while useful, they only describe a particular subset of the responses of these systems. This is in contrast to a nonlinear conservative SDOF system such as $\ddot{x} + x + x^3 = 0$, where all initial conditions will result in a response that falls somewhere on the backbone curve[4]. Therefore, constant amplitude backbones only give limited insight into system behaviour, and tell us nothing about responses where r oscillates.

It may also be verified that Eq. (1) is exactly solved by $\mathbf{x} = r[\cos\omega_r t, \sin\omega_r t]^T$, where ω_r is either ω_f or ω_b from Eq. (9). The same form exactly solves Eq. (3) if ω_r is either $\bar{\omega}_f$ or $\bar{\omega}_b$ from Eq. (10). This confirms that these solutions, which extend from individual modes of the underlying linear system, respond at a single angular velocity regardless of amplitude, and therefore lack the harmonic content required to excite other modes of the system. This gives further demonstration that mode locking is absent in the fully conservative system.

[3]The linearisation around these fixed points is given in Section 5.4.

[4]Backbone curve defined by $\omega_r = \sqrt{1 + \frac{3}{4}X^2}$ for approximate solution $x = X\cos\omega_r t$.

4.2 Critical speed backbone curves

The orbits of greatest interest are usually those that may be excited by the unbalance forcing, and the simplest way that this can occur is when the response is at a constant amplitude, with the angular velocity matching the shaft speed, ie. $\dot{\alpha} = \Omega$. Making this substitution into Eq. (9) gives

$$\omega_f(r,\Omega) \;=\; \Omega \;=\; \frac{\Omega\mu}{2M} + \sqrt{\left(\frac{\Omega\mu}{2M}\right)^2 + \frac{k+k_3r^2}{M}} \qquad \Longrightarrow \qquad \Omega \;=\; \Omega_c(r) \;=\; \sqrt{\frac{k+k_3r^2}{M-\mu}} \tag{11}$$

There are no solutions for $\omega_b(r) = \Omega$ because, as seen in Figure 4 and Eq. (9), $\omega_b(r)$ is negative for an Ω that is assumed positive. Equation (11) gives $\Omega_c(r)$, the amplitude dependent critical speed, or in other words the shaft speed that gives a synchronous whirl at amplitude r. The inverse form

$$r_c(\Omega) = \sqrt{\frac{1}{k_3}\left(\Omega^2(M-\mu) - k\right)} \quad , \quad \Omega \geq \Omega_c(0) \tag{12}$$

gives the amplitude of the conservative system when it whirls at a drivespeed Ω. These results are plotted in Figure 4 (b), and the graph is termed the *critical speed backbone curve*. Synchronous whirling responses of a system with unbalance forcing and damping present, will lie near to the critical speed backbone curve based on the underlying conservative system.

5 Variable amplitude backbone curves

As seen in Section 3, responses of the system will have a varying amplitude r, with the exception of fixed points of Eq. (6). However the majority of these responses are of purely academic interest, because they cannot be excited by the usual form of forcing which for rotating systems is the unbalanced mass. (Compare this to a static structure, where any excitation at a similar frequency to that of a free response is liable to cause a resonant response). The exception are those responses that retain a fixed angular relationship to the unbalance force vector at every cycle, a condition termed *angular synchronisation*[5]. Angular synchronisation is a necessary condition for a response to be excited by unbalance, because if it is not present the forcing will be acting at arbitrary phases to the response, sometimes adding energy and sometimes extracting it from the system, rather than consistently providing the energy that is otherwise dissipated on each cycle in a real system. Angular synchronisation may be equivalently considered as periodicity in the rotating frame. This section uses a mathematical condition to identify angular synchronisation, and then exploits this to draw backbone curves of these responses through a continuation approach. Different types of responses can be found depending on how the branch is initiated, and in some cases further constraints may be applied to identify further conditions of interest. Backbone curves are defined at constant drivespeeds, but are also used to define envelopes of possible responses against drivespeed, in a form comparable to typical bifurcation diagrams for rotating systems.

5.1 The angular synchronisation constraint function

Angular synchronisation occurs when Eq. (8) is satisfied. It emerges that many of the more common responses are found with $p = 1$, with higher values for p related to more complex higher resonances, so henceforth $p = 1$ is assumed unless stated otherwise. However, rather than simply rearranging Eq. (8)

[5]The word angular distinguishes this from the more general concept of synchronisation for dynamical systems. The key difference is that angular synchronisation can be consistently evaluated in any coordinate system. The present argument would struggle if simply based on frequencies because angular velocities, and therefore frequencies, vary under the time varying transformation (2) between stationary and rotating coordinate systems.

to define the constraint function, q is eliminated by defining

$$G(\Psi, T, \Omega) = \text{mod}(p(\Psi - \Omega T) - \pi, 2\pi) - \pi \ , \tag{13}$$

where mod (a, b) returns the remainder of a/b [6]. The zero roots of Eq. (13) will always coincide with a solution of Eq. (8) for some q, with the added numerical benefit that the function has smooth derivatives at these zeros. This form allows continuation to work seamlessly even when q changes along a solution branch, with an example of how this can happen given in Appendix B.

5.2 Evaluating the period and precession angle

As discussed in Section 3, all initial conditions of system (6) lead to periodic responses (except for fixed points), so therefore period and precession angle may be defined as functions of the initial conditions. A phase condition $\dot{r}(0) = 0$ is also assumed, implying without loss of generality that all periods are assumed to start at a maximum or minimum of r over the period. Therefore, functions can be defined that return the period and precession angle of the periodic response associated with initial conditions $r(0) = r_0$ and $\dot{\alpha}(0) = \dot{\alpha}_0$,

$$T = T(r_0, \dot{\alpha}_0, \Omega) \quad , \quad \Psi = \Psi(r_0, \dot{\alpha}_0, \Omega) \ . \tag{14}$$

In the present work, Eq. (14) is evaluated by time simulation of Eq. (5) from the initial condition $\mathbf{y} = [r_0, 0, 0, \dot{\alpha}_0]^T$. Event detection is used to determine the end of the period; as shown in Figure 3(a) the period completes when $\dot{r}$ crosses zero for the second time, moving in the same direction as at $t = 0$. Hence the simulation is terminated when this condition is detected, and T and Ψ are returned[7].

5.3 Continuation framework

Initially, constrained backbones are derived at fixed drivespeeds, in terms of the nonzero initial conditions, giving a continuation problem in the form

$$\mathbf{z} = \begin{bmatrix} r_0 \\ \dot{\alpha}_0 \end{bmatrix} \quad , \quad \mathbf{F}(\mathbf{z}_1) = \begin{bmatrix} G(\Psi(z_1, z_2, \Omega), T(z_1, z_2, \Omega), \Omega) \\ \mathbf{z'}^T(\mathbf{z}_1 - \mathbf{z}_0) - \Delta s \end{bmatrix} = \begin{bmatrix} 0 \\ 0 \end{bmatrix} \ , \tag{15}$$

where $\mathbf{z}_1$ is the solution vector at the present step, z_i is the ith member of $\mathbf{z}_1$, $\mathbf{z}_0$ is the solution at the previous step, $\mathbf{z'}$ is a unit vector indicating the direction of the solution branch, and Δs is the desired step length. The upper part of Eq. (15) ensures that all periodic solutions found meet the angular synchronisation constraint, while the bottom line ensures that the solution progresses in a consistent direction along a solution branch, at a rate controlled by Δs.

In rotordynamics, it is commonly desired to see how dynamic solutions evolve as the drivespeed is varied, in which case the continuation problem becomes

$$\mathbf{z} = \begin{bmatrix} r_0 \\ \dot{\alpha}_0 \\ \Omega \end{bmatrix} \quad , \quad \mathbf{F}(\mathbf{z}_1) = \begin{bmatrix} G(\Psi(z_1, z_2, z_3), T(z_1, z_2, z_3), z_3) \\ H(\Psi, T, \Omega) \\ \mathbf{z'}^T(\mathbf{z}_1 - \mathbf{z}_0) - \Delta s \end{bmatrix} = \begin{bmatrix} 0 \\ 0 \\ 0 \end{bmatrix} \tag{16}$$

where $H(\Psi, T, \Omega)$ is an additional constraint, required to make Eq. (16) a square system, and chosen for various purposes as described in Sections 5.5.1 to 5.5.3.

[6] For example $5 = 3 * 1.4 + 0.8 \implies \text{mod}(5, 1.4) = 0.8$, as implemented by the Matlab® function `mod`.

[7] The approach of using time marching to establish responses is a little similar to the well known shooting method, with the difference that there is no need to perform iterations to establish periodicity, because periodicity is guaranteed for system (6) as discussed in Section 3.1.

Equations (15) and (16) are solved using Newton-Raphson iterations, with all necessary derivatives calculated via a finite-difference approximation. The velocity vector $\mathbf{z}'$ is then updated by solving

$$\left.\frac{\partial \mathbf{F}}{\partial \mathbf{z}}\right|_{\mathbf{z}_1} \mathbf{z}' = \begin{bmatrix}\mathbf{0}\\ 1\end{bmatrix} , \tag{17}$$

after which $\mathbf{z}'$ is rescaled to unit magnitude. The initial value of $\mathbf{z}'$ is chosen on a case by case basis detailed in Sections 5.5.1 to 5.5.3. The stepsize Δs is updated with

$$\Delta s \to \frac{n_{optimal}}{n_{iterations}} \Delta s \tag{18}$$

where $n_{iterations}$ is the number of Newton iterations required to reach tolerance on the step just completed, and $n_{optimal}$ is a desired number of iterations, usually 2 or 3. This allows Δs to seek a compromise between reliable convergence and making reasonable progress along the branch.

5.4 Onset conditions for variable amplitude orbits

The solution branches for variable amplitude orbits originate in one of the two following ways:

1. Linearised small perturbations, satisfying the constraints, about one of the fixed point solutions described in Section 4.

2. Linearised oscillations with r approaching the limit of zero, at particular values of the drivespeed Ω where the linear response satisfies constraints.

The second approach is analysed in Section 5.5.3, while the first is explained here. The Jacobian of $\mathbf{f_a}(\hat{\mathbf{y}})$ given by

$$\frac{\partial \mathbf{f_a}}{\partial \hat{\mathbf{y}}} = \begin{bmatrix} 0 & 1 & 0 \\ \dot{\alpha}^2 - \left(k + 3k_3 r^2 + \mu\Omega\dot{\alpha}\right)/M & 0 & 2r\dot{\alpha} - \mu\Omega r/M \\ \left(2\dot{r}\dot{\alpha} - \mu\Omega\dot{r}/M\right)/r^2 & \left(-2\dot{\alpha} + \mu\Omega/M\right)/r & -2\dot{r}/r \end{bmatrix}$$

is evaluated at a fixed point $\hat{\mathbf{y}}^*$ by substituting Eq. (9) to obtain

$$\mathbf{A} = \begin{bmatrix} 0 & 1 & 0 \\ \dfrac{-2k_3 r^2}{M} & 0 & \dfrac{\pm 2r}{M}\sqrt{\left(\mu\Omega/2\right)^2 + k + k_3 r^2} \\ 0 & -\dfrac{\pm 2}{rM}\sqrt{\left(\mu\Omega/2\right)^2 + k + k_3 r^2} & 0 \end{bmatrix} \tag{19}$$

where the $\pm$ symbol should be taken as $+$ for a fixed point on the forward whirl backbone and $-$ when on the backward whirl backbone. Matrix $\mathbf{A}$ defines the linearised dynamics about the given fixed point; specifically, if the system is slightly perturbed to $\hat{\mathbf{y}} = \hat{\mathbf{y}}^* + \boldsymbol{\Delta}$ the dynamics of small perturbation $\boldsymbol{\Delta}$ are given by $\dot{\boldsymbol{\Delta}} = \mathbf{A}\boldsymbol{\Delta}$.

Matrix $\mathbf{A}$ has three eigenvalues, 0 and $\pm j\omega^*$ where $j = \sqrt{-1}$ and

$$\omega^* = \sqrt{\left(\frac{\mu\Omega}{M}\right)^2 + \frac{2}{M}\left(2k + 3k_3 r^2\right)} . \tag{20}$$

The zero eigenvalue relates to a disturbance that simply moves the system to another adjacent fixed point i.e. along the relevant backbone curve. The remaining conjugate pair of purely imaginary eigenvalues give an oscillation about the fixed point which, like all oscillations for system (6), has a period and precession angle. The period is given by

$$T^*(r, \Omega) = 2\pi/\omega^* , \tag{21}$$

where the asterisk indicates that this period relates to a linearised oscillation about a fixed point. Note that Eq. (20) implies that ω^* and consequently T^* are purely functions of r, regardless of whether the backbone is forward or backward whirling. The precession angle is found by noting that, because the disturbance to $\dot{\alpha}$ is both small and oscillates over period T^*, the average effect on $\dot{\alpha}$ over the period is zero, and hence the overall precession angle of the linearised motion is given by

$$\Psi^*(r,\Omega) = \begin{cases} \Psi_f(r,\Omega) = \omega_f(r,\Omega)T^*(r,\Omega), & \text{for a forward whirl,} \\ \Psi_b(r,\Omega) = \omega_b(r,\Omega)T^*(r,\Omega), & \text{for a backward whirl.} \end{cases} \tag{22}$$

Furthermore, on the critical backbone $\Psi_c(r) = \Psi_f(r,\Omega_c(r))$ may be defined, using (11).

Constraint functions (see Section 5.1) can also be evaluated for linearised oscillations about fixed points to give

$$G^*(r,\Omega) = G(\Psi^*(r,\Omega), T^*(r,\Omega), \Omega) = \begin{cases} G_f(r,\Omega) = G(\Psi_f(r,\Omega), T^*(r,\Omega), \Omega) & \text{on forward whirl backbone,} \\ G_b(r,\Omega) = G(\Psi_b(r,\Omega), T^*(r,\Omega), \Omega) & \text{on backward whirl backbone.} \end{cases} \tag{23}$$

Furthermore, if a forward whirl fixed point is also on the critical speed backbone (see Eq. (11)) $G_c(r) = G_f(r,\Omega_c(r))$ may be defined. If continuing in the form of Eq. (16), similar definitions may be made for $H^*(r,\Omega)$, $H_f(r,\Omega)$, $H_b(r,\Omega)$ and $H_c(r)$.

The condition $G^*(r,\Omega) = 0$, and where relevant $H^*(r,\Omega) = 0$, indicates that a fixed point is the origin for a branch of constrained oscillating amplitude responses. These special fixed points are denoted $\hat{\mathbf{y}}^\dagger = \left[r^\dagger, 0, \dot{\alpha}^\dagger\right]^T$, where $\dot{\alpha}^\dagger$ is found by evaluating either Eqs. (9) or (11) at $r^\dagger$ as appropriate to the type of response under consideration. Values of the solution vector associated with these special points are denoted $\mathbf{z}^\dagger$.

5.5 Particular solutions for different types of variable amplitude orbit

5.5.1 Asynchronous response with one mode directly excited by unbalance

This is a type of response seen in systems with frictional impacts, with examples reported in, for example, [43, 62, 18, 63]. The forward whirling mode is directly excited by the unbalance forcing, whereas some nonlinear force excites in the opposite direction and therefore activates the backward whirl mode. The nonlinear force is typically friction, but here the effect is simply enforced by the chosen constraint. The result is a motion with significant response at the shaftspeed, and at a frequency determined by the backward whirling frequency, and that is generally quasiperiodic in the stationary frame but always periodic in the rotating frame.

Initially, consider the response at a fixed shaft speed $\Omega > \Omega_c(0)$. In order to have a directly excited component, the motion must originate from a fixed point on the critical backbone curve, so

$$\mathbf{z}^\dagger = \begin{bmatrix} r^\dagger \\ \dot{\alpha}^\dagger \end{bmatrix} = \begin{bmatrix} r_c(\Omega) \\ \Omega \end{bmatrix} \tag{24}$$

where $r_c(\Omega)$ is given by Eq. (12), and $\dot{\alpha}_0^\dagger = \omega_f(r^\dagger) = \Omega$.

The initial solution velocity $\mathbf{z}'$ is set by taking the real part of the eigenvectors associated with ω^* (see Eq. (20)) and extracting the r and $\dot{\alpha}$ components, scaling to ensure unit magnitude and a positive r component to induce progress in the direction of increasing amplitude[8]. Continuation in the form of Eq.

[8]This vector can also be found by ensuring that the initial velocity runs normal to the forward whirl backbone curve, to

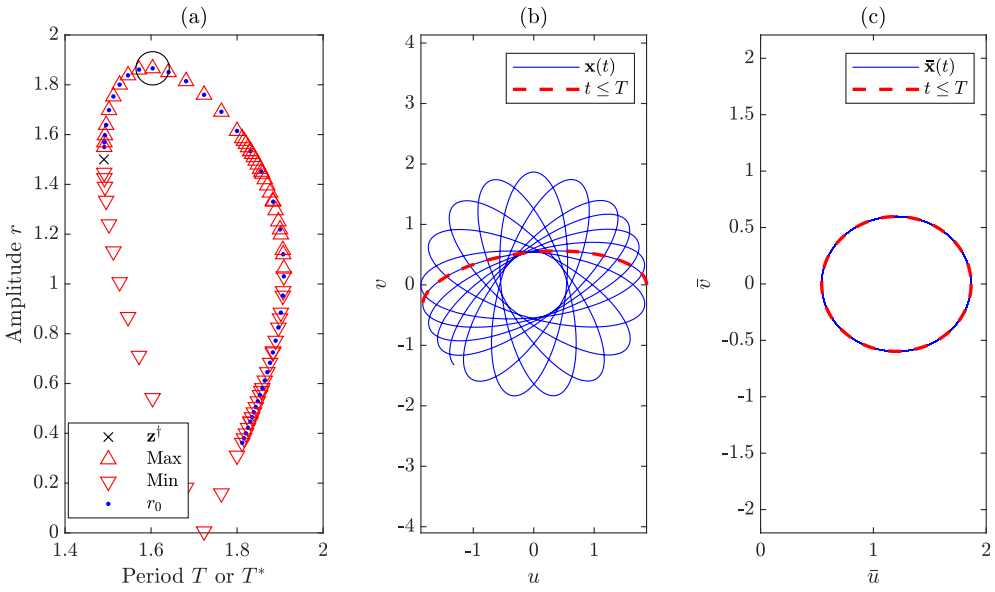

Figure 5: (a) Solutions with constraint equation (13) originating from the critical backbone. (b,c): Flow of the solution marked with a ring ◯ in (a), in stationary and rotating frames respectively.

(15) is then followed.

The results of this are shown in Figure 5, in terms of maximum and minimum r over the cycle and the period T. The maximum amplitude initially rises to a maximum before falling to a point at approximately $T = 1.9$, where the maximum and minimum are the same. At this point, the solution represents infinitesimal oscillations about a fixed point on the backward whirl branch. If the solution continues beyond this point, it finds duplicate responses of those already found, with the difference that the initial condition is now located at the minimum r rather than the maximum. Furthermore, the solver's rate of progress becomes very slow, because as r_0 tends to zero, $\dot{\alpha}_0$ will tend to infinity, causing very small step sizes to become necessary.

A family of solutions similar to the one shown in Figure 5 exists for all points on the critical backbone. The upper bound of these responses can be plotted on a graph against Ω, by solving Eq. (16) with the additional constraint function

$$H(\Psi, T, \Omega) = \frac{\partial G}{\partial \dot{\alpha}_0} \,. \tag{25}$$

This constraint is derived by considering that at the maximum solutions in Figure 5, the term in the velocity $\mathbf{z}'$ relating to r_0 must be zero i.e. $r_0' = 0$. Given that the velocity satisfies

$$\begin{bmatrix} \frac{\partial G}{\partial r_0} & \frac{\partial G}{\partial \dot{\alpha}_0} \end{bmatrix} \begin{bmatrix} r_0' \\ \dot{\alpha}_0' \end{bmatrix} = 0 \,,$$

it can be seen that $r_0' = 0$ when $\frac{\partial G}{\partial \dot{\alpha}_0} = 0$, assuming that $\frac{\partial G}{\partial r_0} \neq 0$ and $\dot{\alpha}_0' \neq 0$.

The origin for the resulting branch of solutions is on the critical backbone curve in the limit of zero amplitude, hence $r_0^\dagger = 0$ and $\dot{\alpha}_0^\dagger = \Omega^\dagger = \Omega_c(0)$. The initial velocity is chosen to be $\mathbf{z}' = [1, 0, 0]^T$, to force r to move away from the singularity that occurs at $r = 0$, while the 2nd constraint function prevents the solution from simply following the critical backbone[9]. The results of this continuation are shown in Figure 6, where a family of solutions similar to those shown in Figure 5 (b) and (c) are seen to exist

ensure that the branch switching occurs.

[9]Note that the condition of zero amplitude represents a singularity in our chosen coordinate system, so this is one of the unusual cases where the continuation algorithm can fail to proceed if the initial step size Δs is too *small*.

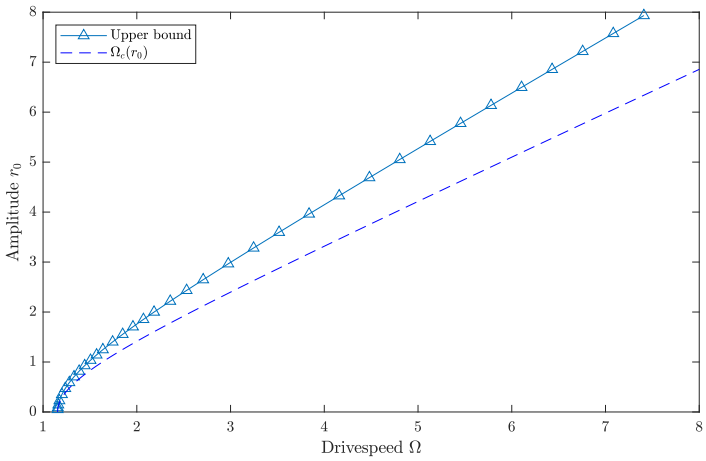

Figure 6: Solution branch satisfying (25), with critical backbone curve added for comparison.

about the critical backbone, originating at the linear critical speed and with maximum amplitude rising monotonically with drive speed.

5.5.2 Synchronous periodic orbits

A special case of the behaviour seen in Section 5.5.1 is when the precession angle $\Psi = \pi$; each period of system (6) performs a half rotation of the origin, and two of these periods completes an approximately elliptical orbit in the stationary frame. In other words, the orbit becomes stationary frame periodic. This type of behaviour is seen where there is some anisotropy to induce stationary frame periodic behaviour, or perhaps a light impact occurs at each time the shaft passes a certain angular position.

To capture this behaviour, a continuation in the form of Eq. (16) is performed, with the additional constraint

$$H(\Psi, T, \Omega) = \Psi - \pi \ , \tag{26}$$

to ensure that the solution is periodic in the stationary frame. The starting point for this branch of solutions lies on the critical speed backbone curve, so Eq. (26) is evaluated for linearised oscillations at the fixed points $\mathbf{z} = [r, \Omega_c(r), \Omega_c(r)]^T$, with the zero point giving $\mathbf{z}^\dagger$. This is illustrated in Figure 7 (a).

The slope of the critical speed backbone in r, Ω space is given by

$$\frac{\mathrm{d}\Omega_c}{\mathrm{d}r} = \frac{k_3}{\sqrt{(k + k_3 r^2)(M - \mu)}} \tag{27}$$

hence the initial direction vector is chosen to be normal to this giving $[\frac{\mathrm{d}\Omega_c}{\mathrm{d}r}, 0, -1]^T$ scaled to unit magnitude.

The results of continuation are shown in Figure 7 (b), showing that at higher amplitudes there are periodic oval shaped responses, despite the absence of anisotropy in the system.

5.5.3 Asynchronous response with no directly excited modes

There is a broad category of orbits that are quasiperiodic in the stationary frame, but are shown to be internally resonant and periodic in the rotating frame [8, 64, 17, 45, 40, 65]. In these orbits, the unbalance force does not directly excite either mode, however the orbits are synchronised to the shaft speed and the modes seem to self-excite. For these orbits, the angular synchronisation condition (13) applies again, however when considering a fixed drive speed Ω, it is seen that the initiation point is on the forward whirl

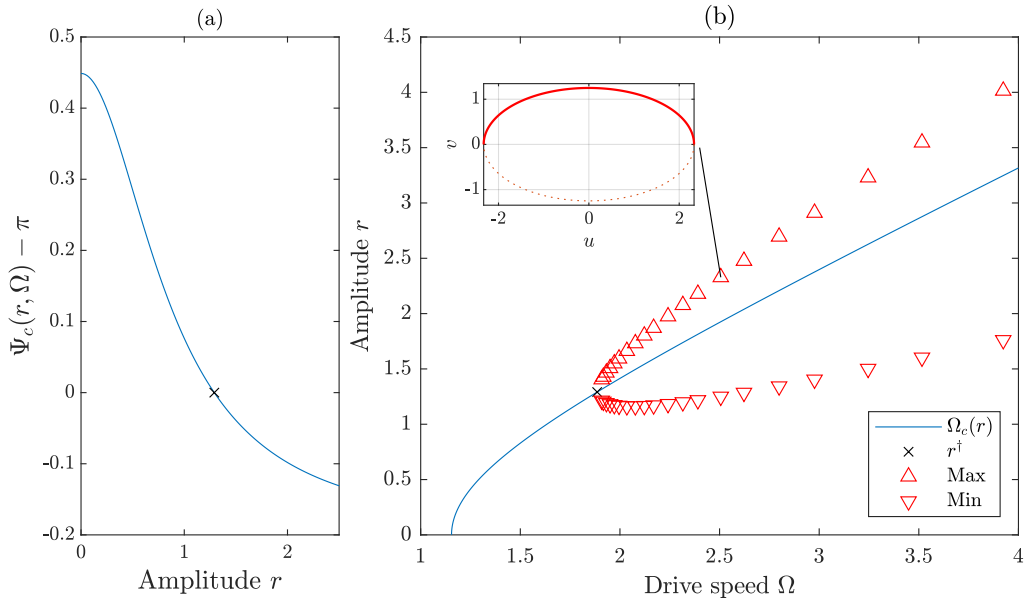

Figure 7: (a) Equation (26) evaluated for linearised oscillations about fixed points on the critical speed backbone curve. (b) Solutions that are both periodic in the stationary frame and synchronised with the drive speed, with the critical speed backbone curve included for comparison.

backbone, rather than the critical speed backbone, reflecting that there is no direct excitation of either mode.

Initially, a fixed drive speed $\Omega = 5$ is considered. The angular synchronisation constraint function (13) is evaluated for small oscillations about the fixed points on the forward whirl backbone given by Eq. (9), and the result of this is shown in Figure 8 (a). The zero crossing of $G_f(r)$ gives $r^\dagger$, and then the starting point for continuation is

$$\mathbf{z}^\dagger = \begin{bmatrix} r^\dagger \\ \dot{\alpha}^\dagger \end{bmatrix} = \begin{bmatrix} r^\dagger \\ \omega_f(r^\dagger) \end{bmatrix} .$$

The continuation is shown in Figure 8. In a similar manner to that seen in Section 5.5.1, the branch initially increases in amplitude, before falling to a fixed point on the backward whirl branch, at which point duplicate responses are found but with the initial condition being a minimum of r rather than a maximum. Figure 9 confirms that responses are quasiperiodic in the stationary frame, and periodic in the rotating frame with a characteristic 'double loop' orbit.

Again, since responses are not unique at a given drivespeed an additional constraint is required to make a meaningful plot on a bifurcation diagram with Ω as an axis. Again, the constraint function (25) is used to locate the maximum possible amplitude of oscillations at each drivespeed. The onset point occurs at amplitude approaching zero, when small oscillations at the linear natural frequencies are seen to satisfy angular synchronisation. This occurs at particular drive speeds, which may be found by evaluating Eq. (10) at $r = 0$ for different Ω, and locating the drive speeds $\Omega^\dagger$ that satisfy

$$n_f \bar{\omega}_f(0, \Omega^\dagger) = n_b \bar{\omega}_b(0, \Omega^\dagger) \tag{28}$$

for integers n_f, n_b, defining an $n_f : n_b$ resonance in the rotating frame [8, 17]. For the present case, $n_f = 1$ and $n_b = 2$. At these drivespeeds, oscillations small enough to be considered linear are guaranteed to form periodic orbits in the rotating frame.

The location of the relevant onset drive speed $\Omega^\dagger$ is shown graphically in Figure 10 (a). The results of continuing in $\mathbf{z} = [r_0, \dot{\alpha}_0, \Omega]^T$ are shown in Figure 10 (b), where it can be seen that the maximal

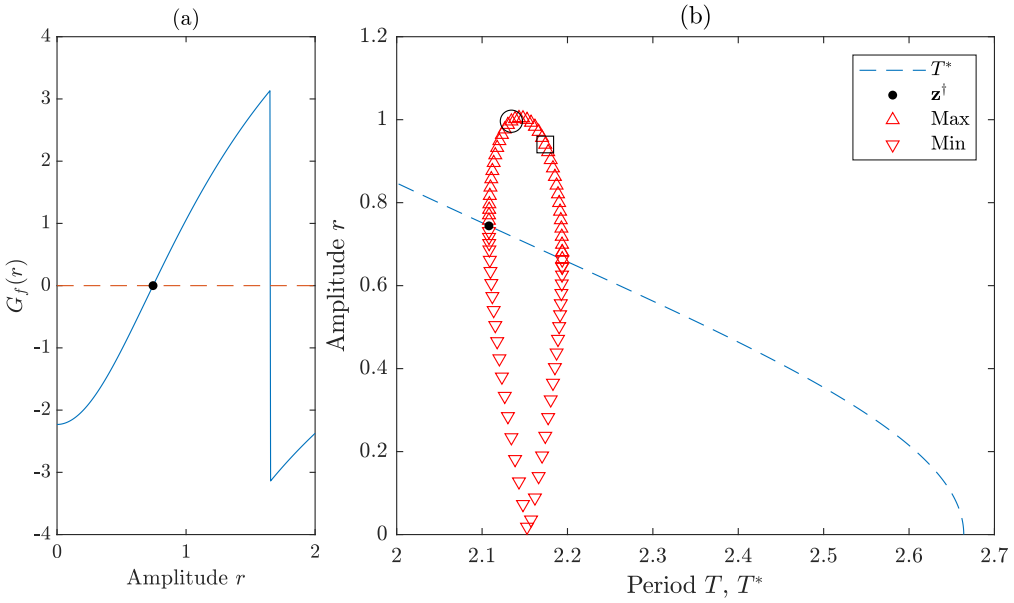

Figure 8: (a) Evaluation of the constraint function (13) for small oscillations about fixed points on the forward whirl backbone curve for $\Omega = 5$. (b) Continuation results for 2:1 responses. Details of the circled solution are given in Figure 9, and the squared and circled solutions are also used as examples for Figure 19 in Appendix 5.1.

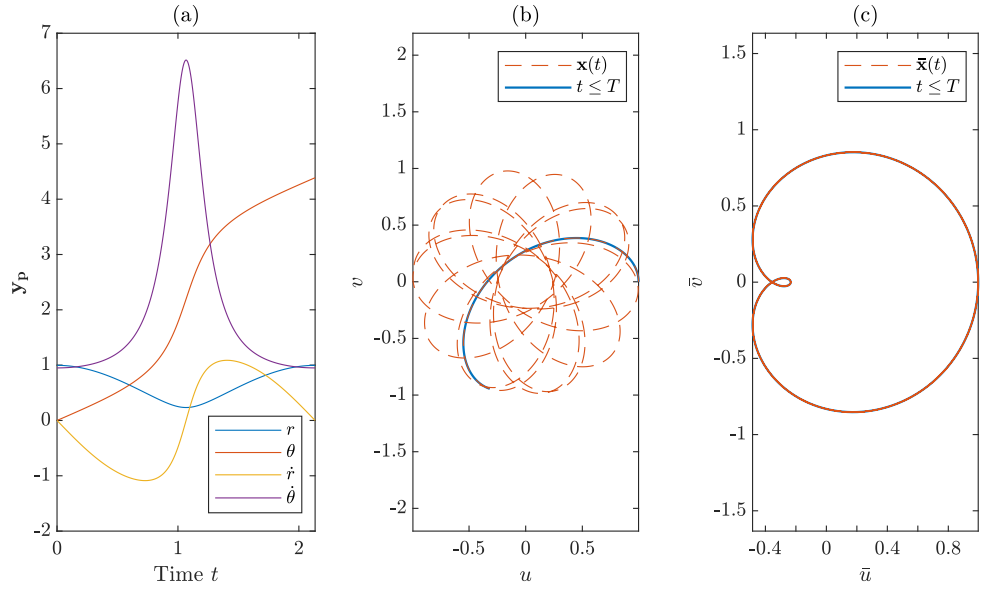

Figure 9: Detail of the solution marked with a circle in Figure 8. (a) Time history of period in polar system. (b,c) Trajectory in stationary and rotating frame coordinates respectively, showing the first 15 periods.

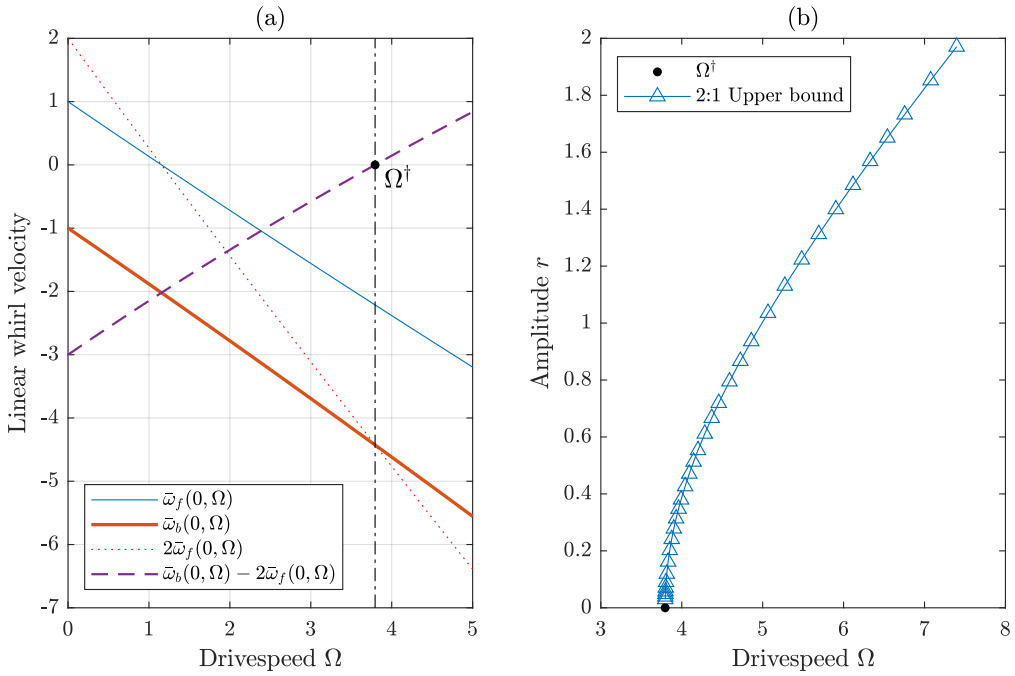

Figure 10: (a) Graphical method for locating the onset drive speed for branch of 2:1 internally resonant asynchronous responses. (b) Continuation results showing the upper bound for 2:1 internally resonant asynchronous responses against drive speed.

amplitude of responses increases steadily with drive speed, and no solutions exist for $\Omega < \Omega^\dagger$.

6 Comparison to forced, damped and weakly anisotropic system responses

In this section, the constrained backbone curves of the conservative isotropic system are compared to responses of systems with non-conservative and anisotropic elements. The non-conservative system responses are extracted with a large number of time simulations, where at each drive speed in a range multiple time simulations are launched with randomised initial conditions. The time simulations are allowed sufficient time to settle, then the final part is assumed to be the steady state condition. The maximum and minimum r from the steady state region is plotted against drive speed Ω, to give a crude impression of the bifurcation diagram for the system. Three different systems are considered, chosen to create different types of nonlinear response. Their time-simulation results are then compared to the results from Section 5 based on the underlying isotropic conservative system to highlight the ability of the constrained backbone analysis to predict potential regions of resonant behaviour.

6.1 Isotropic forced and damped system

In this system, damping and unbalance forcing are added to system (1) to give the stationary frame equation of motion

$$\mathbf{M}\ddot{\mathbf{x}} + (\Omega\mathbf{G} + \mathbf{C})\,\dot{\mathbf{x}} + \mathbf{K}\mathbf{x} + k_3 r^2 \mathbf{x} = M\epsilon\Omega^2 \begin{bmatrix} \cos\Omega t \\ \sin\Omega t \end{bmatrix}, \tag{29}$$

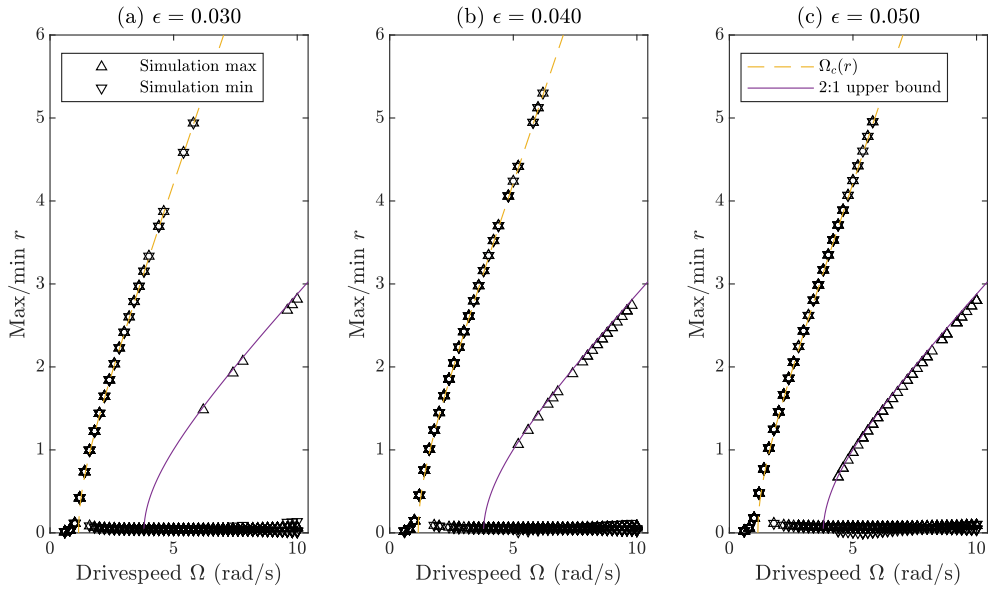

Figure 11: Comparison of an approximate bifurcation diagram found with time simulations, for a forced and damped system with constrained backbones, to the critical backbone and the upper bound for a conservative response with 2:1 resonance in rotating frame.

where $\mathbf{C} = \begin{bmatrix} 0.02 & 0 \\ 0 & 0.02 \end{bmatrix}$, and ϵ represents a small distance between the centre of rotation and the disk mass centre. Other terms are the same as in Eq. (1). Note that forcing terms on the right of Eq. (29) become constant when transformed to the rotating coordinate frame using Eq. (2). Therefore, the unbalance force becomes a constant force vector that breaks the isotropy in the rotating frame, creating a physical means of possibly coupling modes in this frame.

The time simulation results are presented in Figure 11 for varying values of ϵ, with comparison to the critical speed backbone and the upper bound for a 2:1 internally resonant asynchronous response, as analysed in Section 5.5.3. It may be seen that the high amplitude constant amplitude responses fall very near to the critical speed backbone. Similarly, the variable amplitude responses have a maximum amplitude that falls just within the 2:1 upper bound. This shows that system (29) can naturally attract to this mode-locked response, in contrast to the conservative system (1) where it must be enforced through constraints. The level of forcing makes little difference to the amplitudes seen, highlighting that the underlying structure of constrained backbones plays the most important role in shaping the response. However, increasing the forcing level does seem to cause more resonant responses to occur, perhaps by increasing the basin of attraction for these responses. It is interesting that although the 2:1 curve is designed to approximately capture the maximum response, it seems to fall very near to the actual forced response. A possible explanation is that a saturation effect occurs whereby the forcing is sufficient to move the response to near the maximum permitted by the underlying resonance, but cannot increase amplitude further because to do so moves the response away from resonance[10].

It should be noted that the forced and damped responses on the 2:1 branch are isolated from low level responses at all drivespeeds, as confirmed with a more sophisticated method in [21]. However, the present method offers a possible continuation route to these responses, either by considering a fixed drive speed as per Figure 8 and following the conservative forward whirl backbone, or by also continuing in Ω from the onset drivespeed as seen in Figure 10.

[10]Such effects have been reported for nonrotating structures with internal resonance, for example [61, 66] where in some cases large changes in excitation amplitude have relatively small effects on response amplitude.

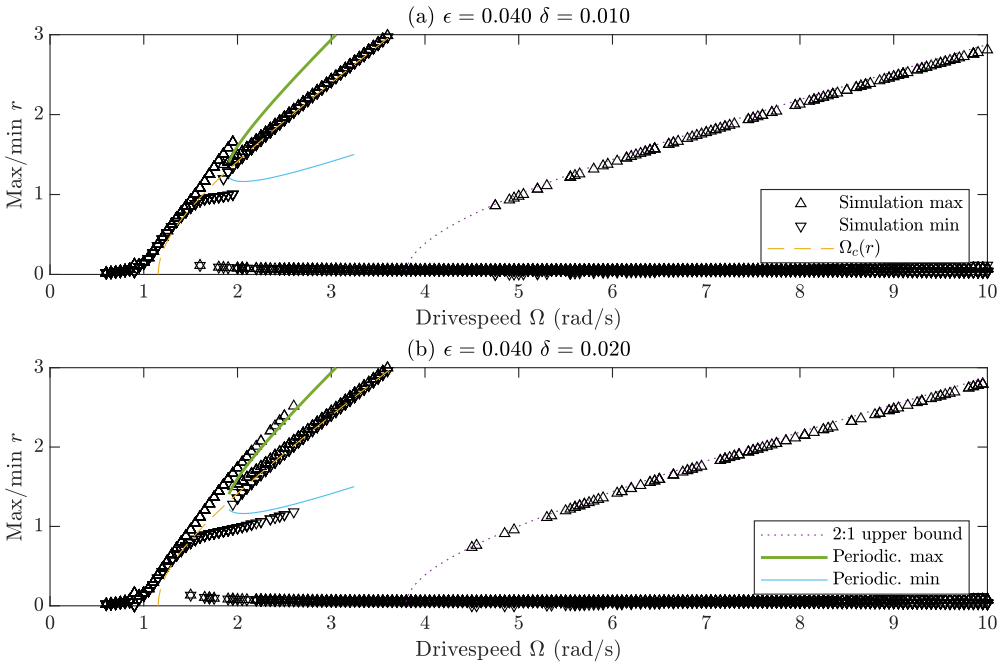

Figure 12: Comparison of an approximate bifurcation diagram found with time simulations, for a weakly anisotropic forced and damped system, to constrained backbones including the critical backbone, the upper bound for 2:1 internal resonance, and the maximum and minimum amplitudes of the periodic variable amplitude response.

6.2 Weakly anisotropic system

In this subsection the system is similar to that presented in Eq. (29), however the stiffness matrix is modified to

$$\mathbf{K} = \begin{bmatrix} k(1+\delta) & 0 \\ 0 & k(1-\delta) \end{bmatrix},$$

where $\delta << 1$. Therefore, the system is weakly anisotropic, but with the mean of the stiffnesses in the x and y directions equal to k to allow straightforward comparisons to system (1).

The introduction of anisotropy leads to the appearance of a new type of response emanating from the primary resonance as shown in Figure 12, and closely following the stationary frame periodic backbone curve studied in Section 5.5.2. It also introduces some smaller oscillations to responses on the constant amplitude critical backbone curve. There is a region where 3 responses are possible; the low amplitude/non resonant response, a response on the critical speed backbone and an oval shaped stationary frame periodic response. Figure 13 shows the orbits of these responses, with a Poincare section marked confirming that these solutions are synchronous with the drive speed. The degree of anisotropy, determined by δ, does not seem to influence the magnitude of the responses very strongly, but does appear to affect their basins of attraction. At other drive speeds, the 2:1 asynchronous response is seen to still occur, highlighting that the same system can exhibit both synchronous and asynchronous responses.

6.3 A pseudo-frictional system

Responses where a single mode is directly excited by unbalance, while the backward whirl responds asynchronously, as discussed in Section 5.5.1, have been seen in frictional impacting systems. These are typically modelled with a piecewise linear stiffness function, rather than a smooth nonlinearity as used here. Piecewise stiffness is beyond the scope of the present study, and for the present purpose

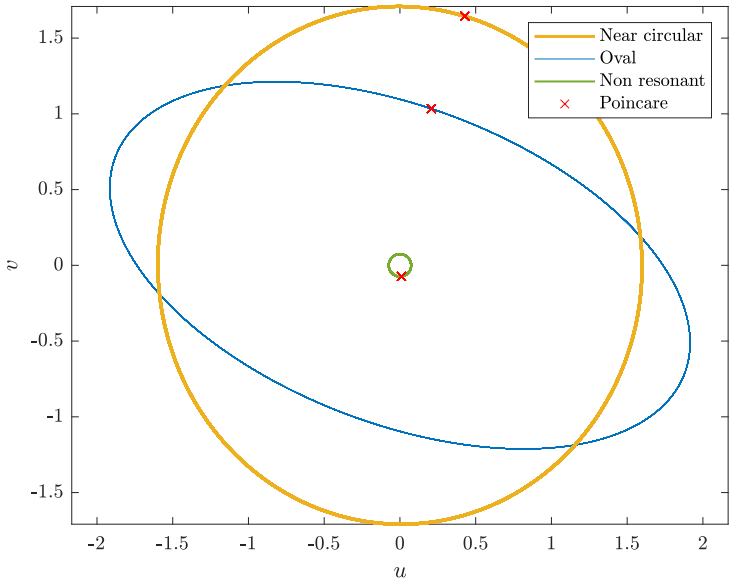

Figure 13: Detail of orbits in the bifurcation diagram in Figure 12 (b), with $\Omega = 2.2$. Poincaré section is taken at time period $2\pi/\Omega$.

maintaining the direct link to the smooth nonlinearity used elsewhere is advantageous. For this reason, the cubic stiffness is retained while a term that behaves similarly to stator friction in a contacting systems, in that it excites the backward whirl mode whenever a certain amplitude is reached, is used in the system definition. The system is given as

$$\mathbf{M}\ddot{\mathbf{x}} + (\Omega\mathbf{G} + \mathbf{C})\,\dot{\mathbf{x}} + \mathbf{K}\mathbf{x} + k_3 r^2 \mathbf{x} + \mathbf{f_c}(\mathbf{x}, \dot{\mathbf{x}}) = M\epsilon\Omega^2 \begin{bmatrix} \cos\Omega t \\ \sin\Omega t \end{bmatrix}, \tag{30}$$

where all terms are as described for Eqs. (1) and (29) except for the pseudo-friction force

$$\mathbf{f_c}(\mathbf{x}, \dot{\mathbf{x}}) = \begin{cases} -c_f \frac{2}{\pi} \arctan\left(\frac{100}{r}\left(u\dot{v} - v\dot{u}\right)\right)(r-a) \begin{bmatrix} -v/r \\ u/r \end{bmatrix} & r \geq a \\ 0 & r < a \end{cases} \tag{31}$$

where c_f is the pseudo-friction coefficient, $r = \sqrt{u^2 + v^2}$, and a is the clearance before friction is encountered. The final vector orients the force in the tangential direction, and the $\frac{2}{\pi}\arctan(\ldots)$ term gives a smoothed approximation to the sign of the tangential velocity of the rotor. While Eq. (30) is not representative of any physical system, it serves the present purpose of highlighting the link between one solution branch for the underlying conservative system and responses of forced dissipative systems.

The results of the time simulations are shown in Figure 14, and it can be seen that the line of maximum asynchronous response gives an approximate guide to many responses. Case (b) shows the type of orbit expected, slightly below the maximum line and with an off-centre near circular orbit in the rotating frame[11]. However it is seen that at the lower drivespeeds, response such a case (a) appear on the other side of the maximal backbone curve. The authors lack a full explanation for this behaviour at present, but note that the rotating frame orbit for case (a) has a winding number of 0, compared to 1 for case (b), suggesting that q has changed in relation (8) (see Appendix B for a little more on this idea). Intruigingly,

[11]Note that it can be shown that the Poincaré section at frequency $\frac{\Omega}{2\pi}$ in the stationary frame traces the orbit in the rotating frame.

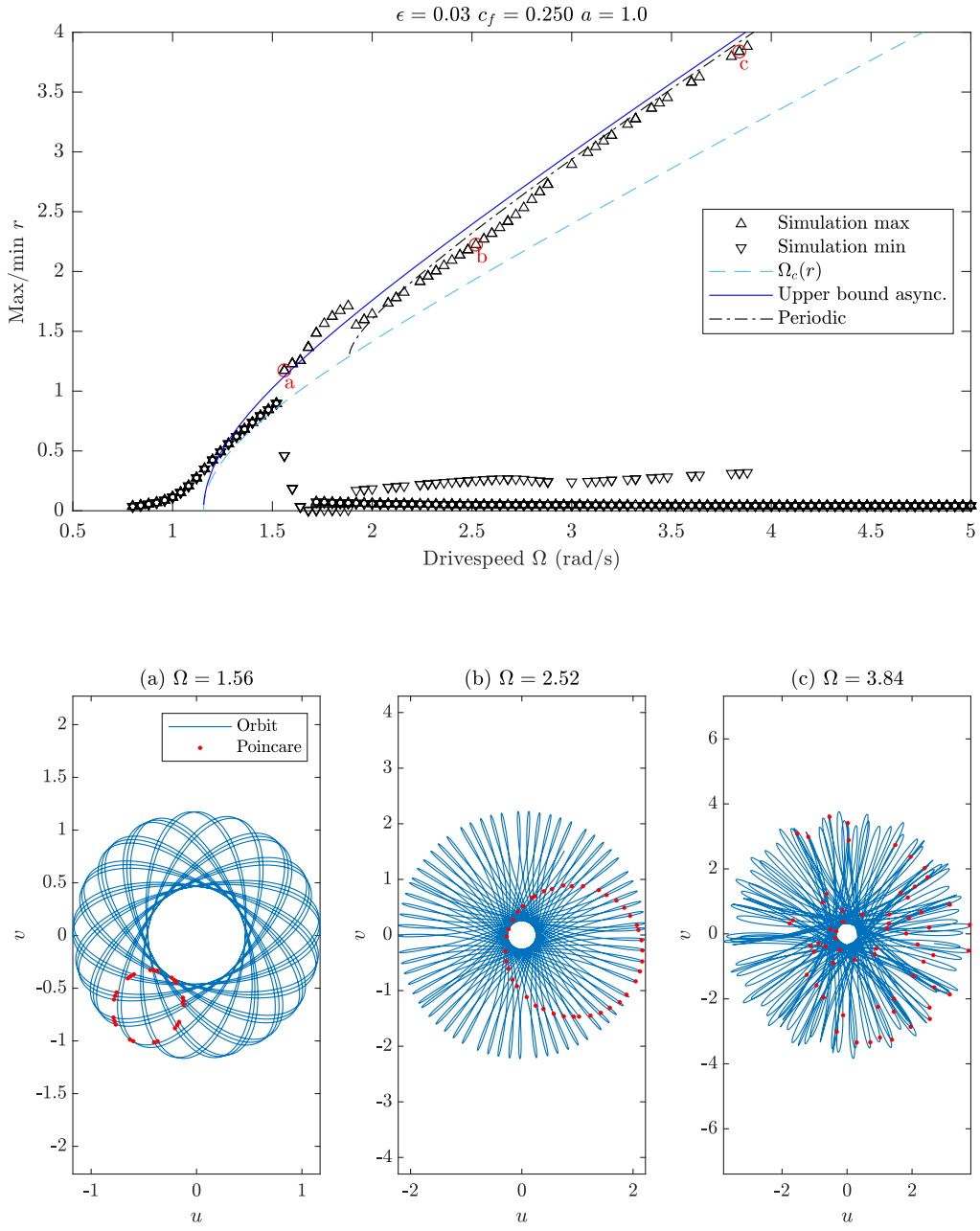

Figure 14: Approximate bifurcation diagram found with time simulations for the system with unbalance forcing and an additional pseudo friction nonlinearity with parameters shown, compared to constrained backbones. Letters indicate where orbits in the subplots below are taken from.

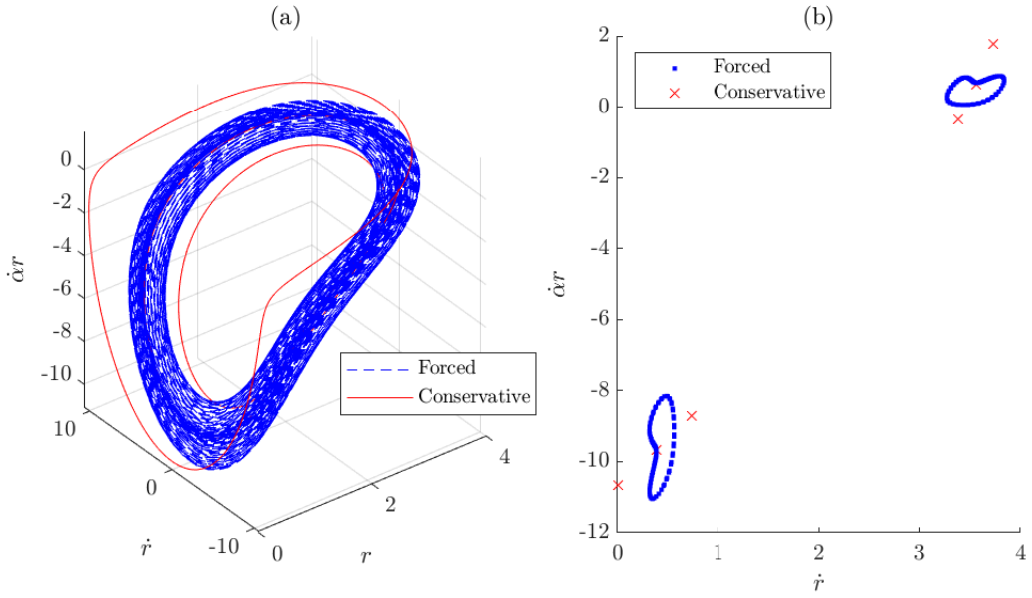

Figure 15: (a) Forced response given in Figure 14 (c) shown in agnostic coordinates, compared to three nearby orbits from the asynchronous backbone curve. (b) Section of orbits taken at $\dot{r} = 0$.

case (c) seems to be chaotic. A full investigation of the complex dynamics of this system is beyond the scope of the present work, however Figure 15 (a) gives an alternative perspective, by representing the forced response in terms of agnostic systems state[12]. This shows that the forced responses are remaining in the vicinity of the underlying conservative responses in the agnostic system as expected. In fact, the response appears to form an approximate torus with associated quasiperiodic behaviour in this frame, with Figure 15 (b) showing an alternate Poincaré projection taken from crossings of the $\dot{r} = 0$ plane, confirming an orbiting behaviour.

7 Comparison to experiment

This section gives a comparison to an experiment, full details of which are given in [67]. Figure 16 shows the test rig which is designed to give a smoothly nonlinear rotating system. A disk is mounted on a slender shaft which is secured at the top by a rigid bearing, and at its lower end to a stator via a bearing, with the stator mounted on four rods with pinned connections. Laser displacement sensors on each side of the stator capture its motion. The disk and stator have approximate mass 2.4kg, and the shaft diameter is 5mm with a distance of approximately 330mm between the upper bearing and the disk. During vibration, the rods give a geometric bend-stretch nonlinearity. Figure 17 shows the results of the experiment in terms of maximum and minimum displacements of steady state responses, where at some drivespeeds the rotor was given manual disturbances to activate the isolated responses. The system is modelled by the four degree of freedom system

$$\bar{\mathbf{M}}\ddot{\bar{\mathbf{x}}} + \left(\bar{\mathbf{C}} + \Omega\bar{\mathbf{G}}\right)\dot{\bar{\mathbf{x}}} + \bar{\mathbf{K}}\bar{\mathbf{x}} + \mathbf{N}(\bar{\mathbf{x}})\bar{\mathbf{x}} = \Omega^2 m_u e\left[\cos(\Omega t), \sin(\Omega t), 0, 0\right]^T \ , \tag{32}$$

[12]In fact, the tangential velocity $\dot{\alpha}r$ has been used in place of the angular velocity $\dot{\alpha}$. This representation gives the same topology but gives a clearer plot, because $\dot{\alpha}$ can take some awkwardly large values.

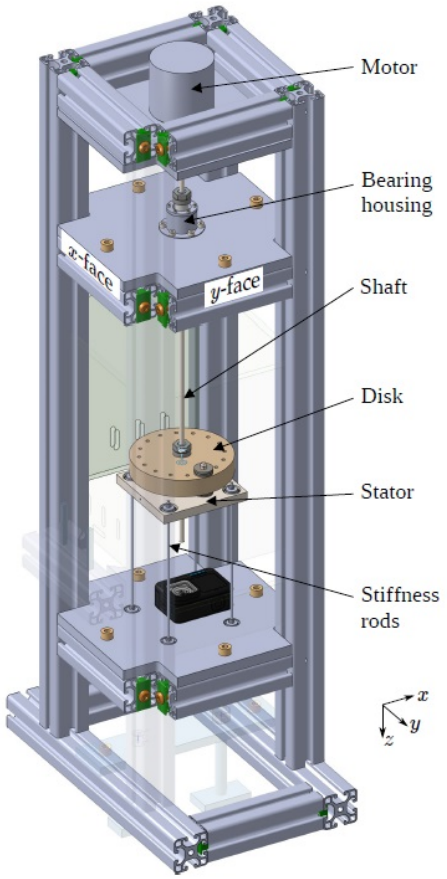

Figure 16: Experimental test rig.

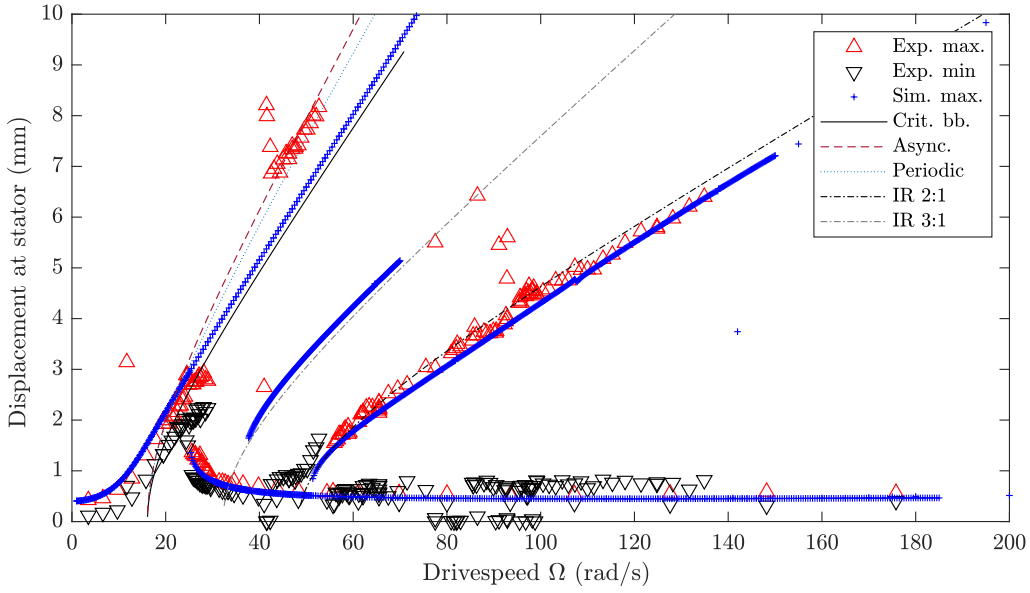

Figure 17: Experimental responses (max and min) compared to time simulation of Eq. (32), and the critical backbone, the upper bound of the directly driven asynchronous response, the periodic backbone, and the upper bounds for 2:1 and 3:1 internally resonant asynchronous responses.

where

$$\bar{\mathbf{M}} = \begin{bmatrix} 2.36 & 0 & 0 & 0.0229 \\ 0 & 2.36 & -0.0229 & 0 \\ 0 & -0.0229 & 0.00234 & 0 \\ 0.0229 & 0 & 0 & 0.00234 \end{bmatrix}, \ \bar{\mathbf{G}} = 10^{-3} \begin{bmatrix} 0 & 0 & 0 & 0 \\ 0 & 0 & 0 & 0 \\ 0 & 0 & 0 & 2.24 \\ 0 & 0 & -2.24 & 0 \end{bmatrix},$$

$$\bar{\mathbf{C}} = \begin{bmatrix} 0.516 & 0 & 0 & 0.0158 \\ 0 & 0.516 & -0.0158 & 0 \\ 0 & -0.0158 & 0.000481 & 0 \\ 0.0158 & 0 & 0 & 0.000481 \end{bmatrix}, \ \bar{\mathbf{K}} = 10^{3} \begin{bmatrix} 2.67 & 0 & 0 & -0.446 \\ 0 & 2.67 & 0.446 & 0 \\ 0 & 0.446 & 0.0992 & 0 \\ -0.446 & 0 & 0 & 0.0992 \end{bmatrix},$$

$$\mathbf{N}(\bar{\mathbf{x}}) = 10^{8}(\bar{x}_1^2 + \bar{x}_2^2) \begin{bmatrix} 1.10 & 0 & 0 & 0.0335 \\ 0 & 1.10 & -0.0335 & 0 \\ 0 & -0.0335 & 0.00102 & 0 \\ 0.0335 & 0 & 0 & 0.00102 \end{bmatrix}, \ m_u e = 8.76 \times 10^{-4} \text{kg m},$$

and $\bar{\mathbf{x}}$ is a four element vector with elements $\bar{x}_i$, where $\bar{x}_1, \bar{x}_2$ are the lateral displacements in meters observed at the stator, and $\bar{x}_3, \bar{x}_4$ are the angular rotations of the disk in radians. Equation (32) is reduced using the modal transform $\bar{\mathbf{x}} = \mathbf{T_r}\mathbf{x}$ where $\mathbf{T_r} = \begin{bmatrix} -0.617 & 0.0365 \\ -0.0365 & -0.617 \\ 0.167 & 2.82 \\ -2.82 & 0.167 \end{bmatrix}$ with columns taken from first two eigenvectors $\mathbf{v}$ of the generalized eigenproblem $\lambda\bar{\mathbf{M}}\mathbf{v} = \bar{\mathbf{K}}\mathbf{v}$. A system in the form of Eq. (1) is then obtained using

$$\mathbf{M} = \mathbf{T_r}^T\bar{\mathbf{M}}\mathbf{T_r} = \begin{bmatrix} 1 & 0 \\ 0 & 1 \end{bmatrix}, \ \mathbf{G} = \mathbf{T_r}^T\bar{\mathbf{G}}\mathbf{T_r},$$

$$\mathbf{K} = \mathbf{T_r}^T\bar{\mathbf{K}}\mathbf{T_r}, \ \mathbf{T_r}^T\bar{\mathbf{N}}\left(\mathbf{T_r}\begin{bmatrix} 1 \\ 0 \end{bmatrix}\right)\mathbf{T_r} = \begin{bmatrix} k_3 & 0 \\ 0 & k_3 \end{bmatrix}.$$

Figure 17 shows the comparison between experiment, and mass time simulations of Eq. (32) and constrained backbones based on the reduced, conservative isotropic form. The time simulations capture the 2:1 branch of the experiment quite well, and approximates some of the main resonance, although it predicts the resonant peak at a much higher amplitude than occurs in the experiment, and does not predict the small oscillations of r that occur near the top of the experimental resonant peak. It makes no prediction of the batch of responses at around 7-8mm in amplitude; these are asynchronous responses, seen in frictional rotor systems such as in [43, 18], and Eq. (32) does not model friction. The simulation also identifies a region of 3:1 internally resonant responses, although experiments only saw occasional responses of this form, with very small basins of attraction and responses typically only lasting for a few moments at a time. There are also some further outlying experimental responses not captured, and these were similarly hard to sustain.

Various constrained backbones are added to Figure 17, matching the majority of responses reasonably closely[13]. Furthermore, the directly driven asynchronous response backbone accurately locates the group of high amplitude responses, not matched by the time simulations. The experimental primary resonance does show some oscillation, again not predicted by system (32), and the oscillations were seen to be periodic in most cases. The fact that the periodic backbone appears at quite a low amplitude would suggest that this behaviour is to be expected.

8 Conclusions

This paper has shown that for a smoothly nonlinear rotordynamic system, simply reducing the system to its underlying conservative elements does not yield the useful insights that this approach achieves for non-rotating structures. However, with additional constraints that anticipate the types of mode locking that occur when unbalance forcing is present, backbone curves are obtained that sit beneath a broad range of forced responses. The constraints are based on the idea of angular synchronisation with the rotating force vector, and the responses predicted can be constant or varying amplitude, periodic or asynchronous. The asynchronous responses occur in two different ways; either the forward whirl mode is

[13]Note that the 3:1 backbone requires the use of $p = 2$ in Eq. (13), following section 5.5.3 with $n_f = 1, n_b = 3$.

directly driven by the unbalance forcing with an asynchronous contribution from the backward whirl, or both modes respond asynchronously in an internally resonant fashion.

The ability to approximately predict where limit cycles of the forced system may occur has been demonstrated both numerically and experimentally, and gives great insight into the potential resonant behaviour of a rotating system without need to calibrate potentially uncertain parameters such as forcing amplitude and damping.

There is much further work to come from this analysis. This includes an extension to the nonsmooth nonlinearity found more widely in real machines, and extension to higher degrees of freedom. Little consideration to the numerical efficiency of the solutions has been given in this work; the present shooting-based solution process has been chosen mainly to provide the most direct implementation of the underlying principles (although the insights gained are found far more rapidly than with time simulations). However, as nonsmooth nonlinearities and more complex rotors come under consideration, efficiency certainly will become more important, and different solution forms such as harmonic balance should be investigated.

Data availability

Data and code for this article are available from `doi.org/10.5281/zenodo.17791695`.

Acknowledgments

Mehmet Akay was supported by the Ministry of National Education of the Republic of Turkey.

Competing interests statement

Financial interests: The authors declare they have no financial interests.
Non-financial interests: Author A. D. Shaw is an editor for Nonlinear Dynamics but will play no part in the processing of this article.

A Proof that flows are periodic in the agnostic system

System (6) is conservative, and therefore any given trajectory is bounded. Furthermore, it possesses time-reversal symmetry, which can be verified by showing that $\mathbf{R}\dot{\hat{\mathbf{y}}} = -\mathbf{f_a}(\mathbf{R}\hat{\mathbf{y}})$ with the involution $\mathbf{R} = \begin{bmatrix} 1 & 0 & 0 \\ 0 & -1 & 0 \\ 0 & 0 & 1 \end{bmatrix}$. The fixed space of $\mathbf{R}$ (satisfying $\mathbf{R}\hat{\mathbf{y}} = \hat{\mathbf{y}}$) is the plane in phase space defined by $\dot{r} = 0$. A theorem of systems possessing time reversal symmetry states that a trajectory that intersects the fixed plane of $\mathbf{R}$ in exactly two positions must be periodic and symmetric about this plane [68].

The fixed points of system (6) are given by Eq. (9), and their eigenvalues are calculated in Eq. (20). The eigenvalue analysis shows that in the phase space near to a fixed point, all states will either be on a trajectory orbiting around the same or an adjacent fixed point, or be another fixed point. Therefore no trajectory can ever reach a fixed point, and inspecting Eq. (6) shows that only fixed points can maintain $\dot{r} = 0$.

With these prerequisites, the proof proceeds by following the flow from a non-fixed point initial condition, which is further assumed to have $\dot{r} > 0$.

- Due to assumption $\dot{r} > 0$, r will increase, and reach a maximum because it must be bounded. This maximum cannot be a fixed point, and will be on the $\dot{r} = 0$ plane because it is a turning point of r.

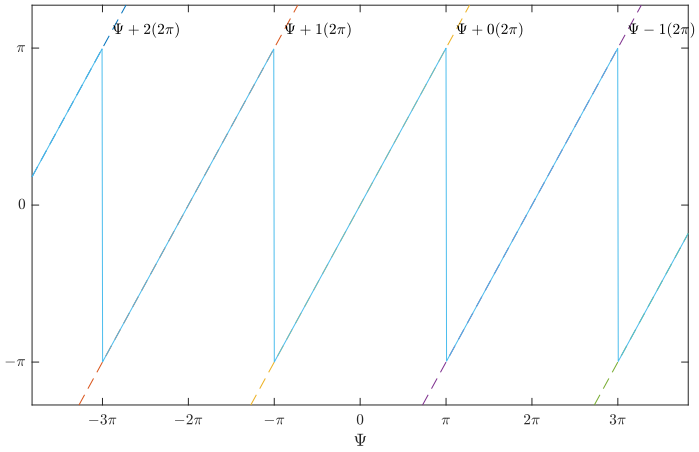

Figure 18: Comparison of $\text{mod}(\Psi - \pi, 2\pi) - \pi$ (13) plotted against $\Psi - 2n\pi$ for different n.

- The flow will therefore follow a trajectory away from the $\dot{r} = 0$ plane that is symmetric with the trajectory that approached it, with $\dot{r} < 0$, until it reaches either a minimum of r or $r = 0$.
- If a minimum is reached, it cannot be a fixed point and must be on the $\dot{r} = 0$ plane. Therefore it will continue on a mirrored trajectory, back towards the previously encountered maximum, fulfilling the requirement of passing twice through the symmetry plane proving that the motion is periodic.

The problem of a trajectory that reaches $r = 0$ cannot be directly handled by considering Eq. (6) due to the polar singularity. However, briefly using the system definition in the form of Eq. (1), it can be shown that in physical terms there are no complex dynamics at this point. Consider a point $\mathbf{x}_-$ that is infinitesimally close to the origin, on a flow that is about to pass directly through the origin, with velocity $\dot{\mathbf{x}}_-$ that is oriented directly towards the origin. Immediately after passing through the origin the flow will reach $\mathbf{x}_+ = -\mathbf{x}_-$, but its velocity will be unchanged i.e. $\dot{\mathbf{x}}_+ = \dot{\mathbf{x}}_-$. Mapping these to agnostic quantities using (4) gives $r_+ = r_-$, $\dot{r}_+ = -\dot{r}_-$ and $\dot{\alpha}_+ = -\dot{\alpha}_- = 0$, where condition $\dot{\alpha} = 0$ is necessary for the trajectory to pass through the origin. Therefore, passing through $r = 0$ simply continues on a mirrored orbit like any other flow passing through the $\dot{r} = 0$ plane, and is therefore also periodic.

B More detail on the angular synchronisation indicator

Figure 18 shows how the form of the angular synchronisation function (with $p = 1$, with reference to (13)) transforms an angle Ψ, whilst aligning at all times with lines of $\Psi - 2q\pi$. It also shows how zeros are maintained, and that gradients at zeros remain smooth.

Figure 19 shows why this is necessary; two orbits that are reasonably near to each other on the same branch shown in Figure 8 have substantially different precession angles. As Figure 19 (a) shows, their stationary frame trajectories take different sides of the origin, causing one to have a positive precession angle while the other's is negative. If both orbits had paths that passed infinitesimally close, but still either side, of the origin, it can be seen that their start and end points would be infinitesimally close together, and there would be a difference approaching 2π in their respective precession angles. In Figure 19 (b), it is seen that this also relates to a change in the winding number of their rotating frame orbits, defined by the number of complete rotations about the origin [69], from 1 to 2. Without the chosen form of angular synchronisation indicator function, these discontinuities in the precession angle and consequently the constraint function would cause the gradient based solutions to fail.

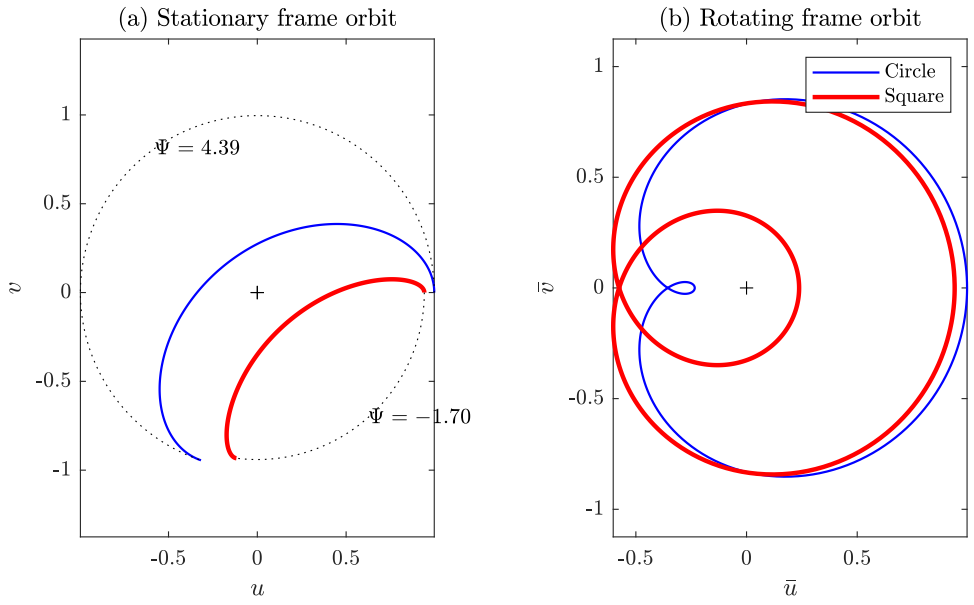

Figure 19: Two orbits taken from the branch shown in Figure 8.

References

[1] M. I. Friswell, J. E. T. Penny, S. D. Garvey, and A. W. Lees, *Dynamics of Rotating Machines*. Cambridge, 2010.

[2] W. Jung, L. S. Andrés, and J. Kim, "A nonlinear rotordynamics model for automotive turbochargers coupled to a physical model for a (semi) floating ring bearing system," *Journal of Engineering for Gas Turbines and Power*, vol. 144, no. 11, p. 111002, 2022.

[3] A. Paiva, R. V. Moreira, A. Brandão, and M. A. Savi, "Nonlinear dynamics of a rotor–stator system with contacts," *Nonlinear Dynamics*, vol. 111, no. 13, pp. 11753–11772, 2023.

[4] A. Fasihi, M. Shahgholi, G. Kudra, M. GhandchiTehrani, and J. Awrejcewicz, "The influence of rotor-stator contact on the nonlinear vibration of an asymmetrical rotor: A. fasihi et al.," *Nonlinear Dynamics*, vol. 113, no. 20, pp. 27435–27457, 2025.

[5] H. Guan, J. Li, K. Wei, and H. Zou, "Rotordynamics of a rotor radially and axially supported by active bump-type foil bearings and bump-type thrust foil bearings," *Mechanical Systems and Signal Processing*, vol. 208, p. 110995, 2024.

[6] J. Taghipour, M. Dardel, and M. H. Pashaei, "Nonlinear vibration mitigation of a flexible rotor shaft carrying a longitudinally dispositioned unbalanced rigid disc," *Nonlinear Dynamics*, vol. 104, no. 3, pp. 2145–2184, 2021.

[7] H. Zhu, H. Jiao, Q. Chen, and L. Fan, "Dynamic analysis of supercritical multispan rotor system with flexible connections and elastic supports," *International Journal of Rotating Machinery*, vol. 2025, no. 1, p. 6690548, 2025.

[8] A. Zilli, R. J. Williams, and D. J. Ewins, "Nonlinear dynamics of a simplified model of an overhung rotor subjected to intermittent annular rubs," *Journal of Engineering for Gas Turbines and Power*, vol. 137, no. 6, p. 065001, 2015.

[9] F. F. Ehrich, "The dynamic stability of rotor/stator radial rubs in rotating machinery," *Journal of Engineering for Industry*, vol. 91, no. 4, pp. 1025–1028, 1969.

[10] J. Yang, D. Shin, and A. Palazzolo, "Fourier neural operator for flow-induced rotordynamics force prediction and application to a sco2 magnetic bearing-rotor system," *Mechanical Systems and Signal Processing*, vol. 232, p. 112750, 2025.

[11] H. Xu, C. Shao, B. Yang, and Q. An, "Numerical investigation on the rotordynamics of a high-speed air compressor supported by gas foil bearings," *Proceedings of the Institution of Mechanical Engineers, Part C: Journal of Mechanical Engineering Science*, vol. 238, no. 12, pp. 5580–5596, 2024.

[12] L. Cui and J. Zheng, "Nonlinear vibration and stability analysis of a flexible rotor supported on angular contact ball bearings," *Journal of Vibration and Control*, vol. 20, no. 12, pp. 1767–1782, 2014.

[13] S. P. Harsha, "Nonlinear dynamic analysis of an unbalanced rotor supported by roller bearing," *Chaos, Solitons & Fractals*, vol. 26, no. 1, pp. 47–66, 2005.

[14] Y. Cui and Y. Wang, "Effect of disk flexibility on nonlinear vibration characteristics of shaft-disk rotors," *Acta Mechanica Sinica*, vol. 40, no. 3, p. 523140, 2024.

[15] Y. Ishida, I. Nagasaka, T. Inoue, and S. Lee, "Forced oscillations of a vertical continuous rotor with geometric nonlinearity," *Nonlinear dynamics*, vol. 11, no. 2, pp. 107–120, 1996.

[16] Y. Ishida and T. Yamamoto, *Linear And Nonlinear Rotordynamics: a modern treatment with applications*. John Wiley & Sons, 2013.

[17] A. D. Shaw, A. R. Champneys, and M. I. Friswell, "Asynchronous partial contact motion due to internal resonance in multiple degree-of-freedom rotordynamics," *Proc. R. Soc. A*, vol. 472, no. 2192, p. 20160303, 2016.

[18] E. Chipato, A. D. Shaw, and M. I. Friswell, "Frictional effects on the nonlinear dynamics of an overhung rotor," *Communications in Nonlinear Science and Numerical Simulation*, vol. 78, p. 104875, 2019.

[19] M. Stender and N. Hoffmann, "bstab: an open-source software for computing the basin stability of multi-stable dynamical systems," *Nonlinear dynamics*, vol. 107, no. 2, pp. 1451–1468, 2022.

[20] Z. Liu, X. He, Z. Ding, and Z. Zhang, "A basin stability based metric for ranking the transient stability of generators," *IEEE Transactions on Industrial Informatics*, vol. 15, no. 3, pp. 1450–1459, 2018.

[21] M. S. Akay, A. D. Shaw, and M. I. Friswell, "Continuation analysis of a nonlinear rotor system," *Nonlinear Dynamics*, vol. 105, no. 1, pp. 25–43, 2021.

[22] M. S. Akay, A. D. Shaw, and M. I. Friswell, "Continuation analysis of overhung rotor bouncing cycles with smooth and contact nonlinearities," *International Journal of Non-Linear Mechanics*, vol. 150, p. 104343, 2023.

[23] F. F. Ehrich and J. O'Connor, "Stator whirl with rotors in bearing clearance," *Journal of Engineering for Industry*, vol. 89, no. 3, pp. 381–389, 1967.

[24] F. F. Ehrich, "Sum and difference frequencies in vibration of high speed rotating machinery," *Journal of Engineering for Industry*, vol. 94, no. 1, pp. 181–184, 1972.

[25] F. F. Ehrich, "High order subharmonic response of high speed rotors in bearing clearance," *Journal of Vibration, Acoustics, Stress, and Reliability in Design*, vol. 110, no. 1, pp. 9–16, 1988.

[26] F. F. Ehrich, "Observations of nonlinear phenomena in rotordynamics," *Journal of System Design and Dynamics*, vol. 2, no. 3, pp. 641–651, 2008.

[27] Y. Ishida and T. Inoue, "Nonstationary oscillations of a nonlinear rotor during acceleration through the major critical speed: influence of internal resonance (special issue on nonlinear dynamics)," *JSME International Journal Series C Mechanical Systems, Machine Elements and Manufacturing*, vol. 41, no. 3, pp. 599–607, 1998.

[28] Y. Ishida and T. Inoue, "Internal resonance phenomena of the jeffcott rotor with nonlinear spring characteristics," *Journal of Vibration and Acoustics*, vol. 126, no. 4, pp. 476–484, 2004.

[29] Y. Ishida and T. Inoue, "Internal resonance phenomena of an asymmetrical rotating shaft," *Modal Analysis*, vol. 11, no. 9, pp. 1173–1193, 2005.

[30] T. Inoue and Y. Ishida, "Chaotic vibration and internal resonance phenomena in rotor systems," *Journal of Vibration and Acoustics*, vol. 128, no. 2, pp. 156–169, 2006.

[31] A. Muszyńska, *Rotordynamics*. CRC press, 2005.

[32] R. D. Neilson and A. D. S. Barr, "Dynamics of a rigid rotor mounted on discontinuously nonlinear elastic supports," *Proceedings of the Institution of Mechanical Engineers, Part C: Journal of Mechanical Engineering Science*, vol. 202, no. 5, pp. 369–376, 1988.

[33] W. Szczygielski, "Application of chaos theory to the contacting dynamics of high-speed rotors," *Rotating machinery dynamics*, pp. 319–326, 1987.

[34] F. Chu and Z. Zhang, "Bifurcation and chaos in a rub-impact jeffcott rotor system," *Journal of Sound and Vibration*, vol. 210, no. 1, pp. 1–18, 1998.

[35] E. V. Karpenko, M. Wiercigroch, and M. P. Cartmell, "Regular and chaotic dynamics of a discontinuously nonlinear rotor system," *Chaos, Solitons & Fractals*, vol. 13, no. 6, pp. 1231–1242, 2002.

[36] Y. Kim, S. Noah, and Y. Choi, "Periodic response of multi-disk rotors with bearing clearances," *Journal of sound and vibration*, vol. 144, no. 3, pp. 381–395, 1991.

[37] Y.-B. Kim and S. Noah, "Quasi-periodic response and stability analysis for a non-linear jeffcott rotor," *Journal of Sound and Vibration*, vol. 190, no. 2, pp. 239–253, 1996.

[38] G. von Groll and D. J. Ewins, "The harmonic balance method with arc-length continuation in rotor/stator contact problems," *Journal of sound and vibration*, vol. 241, no. 2, pp. 223–233, 2001.

[39] L. Salles, B. Staples, N. Hoffmann, and C. Schwingshackl, "Continuation techniques for analysis of whole aeroengine dynamics with imperfect bifurcations and isolated solutions," *Nonlinear Dynamics*, vol. 86, no. 3, pp. 1897–1911, 2016.

[40] A. D. Shaw, A. R. Champneys, and M. I. Friswell, "Normal form analysis of bouncing cycles in isotropic rotor stator contact problems," *International Journal of Mechanical Sciences*, vol. 155, pp. 83–97, 2019.

[41] L. Peletan, S. Baguet, M. Torkhani, and G. Jacquet-Richardet, "Quasi-periodic harmonic balance method for rubbing self-induced vibrations in rotor–stator dynamics," *Nonlinear Dynamics*, vol. 78, no. 4, pp. 2501–2515, 2014.

[42] G. H. van der Heijden, "Mode-locking in nonlinear rotordynamics," *Journal of Nonlinear Science*, vol. 5, no. 3, pp. 257–283, 1995.

[43] M. O. T. Cole and P. S. Keogh, "Asynchronous periodic contact modes for rotor vibration within an annular clearance," *Proceedings of the Institution of Mechanical Engineers, Part C: Journal of Mechanical Engineering Science*, vol. 217, no. 10, pp. 1101–1115, 2003.

[44] P. S. Keogh and M. O. T. Cole, "Rotor vibration with auxiliary bearing contact in magnetic bearing systems part 1: Synchronous dynamics," *Proceedings of the Institution of Mechanical Engineers, Part C: Journal of Mechanical Engineering Science*, vol. 217, no. 4, pp. 377–392, 2003.

[45] K. Mora, A. R. Champneys, A. D. Shaw, and M. I. Friswell, "Explanation of the onset of bouncing cycles in isotropic rotor dynamics; a grazing bifurcation analysis," *Proceedings of the Royal Society A*, vol. 476, no. 2237, p. 20190549, 2020.

[46] G. Kerschen, M. Peeters, J.-C. Golinval, and A. F. Vakakis, "Nonlinear normal modes, part i: A useful framework for the structural dynamicist," *Mechanical Systems and Signal Processing*, vol. 23, no. 1, pp. 170 – 194, 2009. Special Issue: Non-linear Structural Dynamics.

[47] M. Peeters, R. Viguié, G. Sérandour, G. Kerschen, and J.-C. Golinval, "Nonlinear normal modes, part ii: Toward a practical computation using numerical continuation techniques," *Mechanical systems and signal processing*, vol. 23, no. 1, pp. 195–216, 2009.

[48] C. Touzé, A. Vizzaccaro, and O. Thomas, "Model order reduction methods for geometrically nonlinear structures: a review of nonlinear techniques," *Nonlinear Dynamics*, vol. 105, no. 2, pp. 1141–1190, 2021.

[49] M. Legrand, D. Jiang, C. Pierre, and S. W. Shaw, "Nonlinear normal modes of a rotating shaft based on the invariant manifold method," *International Journal of Rotating Machinery*, vol. 10, no. 4, p. 419761, 2004.

[50] T. Wang and Q. Ding, "Nonlinear normal modes and dynamic balancing for a nonlinear rotor system," *Nonlinear Dynamics*, vol. 112, no. 13, pp. 10823–10844, 2024.

[51] S. Wang, L. Hong, and J. Jiang, "Evaluation on spectral submanifold based reduced models of a rotor/stator rubbing system with cross-coupling stiffness," *International Journal of Mechanical Sciences*, vol. 228, p. 107486, 2022.

[52] E. Pesheck, C. Pierre, and S. W. Shaw, "Modal reduction of a nonlinear rotating beam through nonlinear normal modes," *J. Vib. Acoust.*, vol. 124, no. 2, pp. 229–236, 2002.

[53] P. Apiwattanalunggarn, S. W. Shaw, C. Pierre, and D. Jiang, "Finite-element-based nonlinear modal reduction of a rotating beam with large-amplitude motion," *Journal of Vibration and Control*, vol. 9, no. 3-4, pp. 235–263, 2003.

[54] A. Martin, A. Opreni, A. Vizzaccaro, M. Debeurre, L. Salles, A. Frangi, O. Thomas, and C. Touzé, "Reduced-order modeling of geometrically nonlinear rotating structures using the direct parametrisation of invariant manifolds," *Journal of Theoretical, Computational and Applied Mechanics*, 2023.

[55] A. Mereles, D. S. Alves, and K. L. Cavalca, "Model reduction of rotor-foundation systems using the approximate invariant manifold method," *Nonlinear Dynamics*, vol. 111, no. 12, pp. 10743–10768, 2023.

[56] A. Mereles, D. S. Alves, and K. L. Cavalca, "Bifurcations and limit cycle prediction of rotor systems with fluid-film bearings using center manifold reduction," *Nonlinear Dynamics*, vol. 111, no. 19, pp. 17749–17767, 2023.

[57] G. Schmidt and A. Tondl, *Non-linear vibrations*, vol. 66. Walter de Gruyter GmbH & Co KG, 1986.

[58] K. Worden and G. R. Tomlinson, *Nonlinearity in Structural Dynamics*. Bristol: Institute of Physics, 2001.

[59] A. Cammarano, T. L. Hill, S. A. Neild, and D. J. Wagg, "Bifurcations of backbone curves for systems of coupled nonlinear two mass oscillator," *Nonlinear Dynamics*, vol. 77, no. 1-2, pp. 311–320, 2014.

[60] T. L. Hill, A. Cammarano, S. A. Neild, and D. J. Wagg, "Interpreting the forced responses of a two-degree-of-freedom nonlinear oscillator using backbone curves," *Journal of Sound and Vibration*, vol. 349, pp. 276–288, 2015.

[61] A. D. Shaw, T. L. Hill, S. A. Neild, and M. I. Friswell, "Periodic responses of a structure with 3: 1 internal resonance," *Mechanical Systems and Signal Processing*, vol. 81, pp. 19–34, 2016.

[62] K. Mora, C. Budd, P. Glendinning, and P. Keogh, "Non-smooth Hopf-type bifurcations arising from impact-friction contact events in rotating machinery," *Proc. Roy. Soc. Lond. A*, vol. 470, p. art. no. 20140490, 2014.

[63] E. T. Chipato, A. D. Shaw, M. I. Friswell, and R. Sánchez Crespo, "Experimental study of rotor-stator contact cycles," *Journal of Sound and Vibration*, vol. 502, p. 116097, 2021.

[64] Y. Ishida, M. Inagaki, R. Ejima, and A. Hayashi, "Nonlinear resonances and self-excited oscillations of a rotor caused by radial clearance and collision," *Nonlinear Dynamics*, vol. 57, no. 4, pp. 593–605, 2009.

[65] E. Chipato, A. D. Shaw, and M. I. Friswell, "Effect of gravity-induced asymmetry on the nonlinear vibration of an overhung rotor," *Communications in Nonlinear Science and Numerical Simulation*, vol. 62, pp. 78–89, 2018.

[66] T. Detroux, J.-P. Noël, L. N. Virgin, and G. Kerschen, "Experimental study of isolas in nonlinear systems featuring modal interactions," *PloS one*, vol. 13, no. 3, 2018.

[67] M. S. Akay, *Nonlinear Interactions in Rotordynamics*. PhD thesis, Swansea University, 2025.

[68] J. S. Lamb and J. A. Roberts, "Time-reversal symmetry in dynamical systems: a survey," *Physica D: Nonlinear Phenomena*, vol. 112, no. 1-2, pp. 1–39, 1998.

[69] E. W. Weisstein, *CRC concise encyclopedia of mathematics*. Chapman and Hall/CRC, 2002.